

RESEARCH ARTICLE

A clinically relevant model of acute respiratory distress syndrome in human-size swine

Sarah R. Kaslow^{1,2,*}, Jonathan A. Reimer^{1,2,3,*}, Meghan R. Pinezich², Maria R. Hudock^{2,4}, Panpan Chen^{1,2}, Mariya G. Morris⁵, Mandy L. Kain⁵, Jay S. Leb⁶, Carrie B. Ruzal-Shapiro⁶, Charles C. Marboe⁷, Matthew Bacchetta⁸, N. Valerio Dorrello⁹ and Gordana Vunjak-Novakovic^{2,10,‡}

ABSTRACT

Despite over 30 years of intensive research for targeted therapies, treatment of acute respiratory distress syndrome (ARDS) remains supportive in nature. With mortality upwards of 30%, a high-fidelity pre-clinical model of ARDS, on which to test novel therapeutics, is urgently needed. We used the Yorkshire breed of swine to induce a reproducible model of ARDS in human-sized swine to allow the study of new therapeutics, from both mechanistic and clinical standpoints. For this, animals were anesthetized, intubated and mechanically ventilated, and pH-standardized gastric contents were delivered bronchoscopically, followed by intravenous infusion of *Escherichia coli*-derived lipopolysaccharide. Once the ratio of arterial oxygen partial pressure (PaO₂) to fractional inspired oxygen (F_IO₂) had decreased to <150, the animals received standard ARDS treatment for up to 48 h. All swine developed moderate to severe ARDS. Chest radiographs taken at regular intervals showed significantly worse lung edema after induction of ARDS. Quantitative scoring of lung injury demonstrated time-dependent increases in interstitial and alveolar edema, neutrophil infiltration, and mild to moderate alveolar membrane thickening. This pre-clinical model of ARDS in human-sized swine recapitulates the clinical, radiographic and histopathologic manifestations of ARDS, providing a tool to study therapies for this highly morbid lung disease.

KEY WORDS: Animal model, Lung, Inflammation, Systemic, Pathophysiology, Pulmonary function

INTRODUCTION

Acute respiratory distress syndrome (ARDS) is a highly lethal pattern of lung injury, with hospital mortality rates of 35–46%, depending on severity (Bellani et al., 2016). Despite more than 30 years of clinical trials, targeted therapeutics with proven mortality benefits remain elusive (Matthay et al., 2017; Shaw et al., 2019). Evidence to support adjunctive treatments, including extracorporeal membrane oxygenation (Combes et al., 2018; Peek et al., 2009), have remained equivocal. Thus, the treatment of ARDS is supportive in nature, relying on therapies aimed at improving ventilation and oxygenation, and limiting further lung damage, such as lung protective ventilation (Acute Respiratory Distress Syndrome Network et al., 2000), prone positioning and neuromuscular blockade (Papazian et al., 2010) while waiting for the patient to recover. Examining novel, targeted therapeutics, from both mechanistic and clinical standpoints, using a pre-clinical model with direct clinical relevance, therefore, remains a research priority for the National Heart, Lung, and Blood Institute (NHLBI) and American Thoracic Society (ATS) (Semler et al., 2020; Shaw et al., 2019).

The precise clinical criteria of ARDS diagnosis provided by the Berlin Definition (ARDS Definition Task Force et al., 2012) (Table S1), routinely used clinically and applied to human-sized models, allows for critical evaluation of animal models for clinical relevance. Key features of an experimental model of acute lung injury in animals include (1) rapid onset after the inciting event, (2) strong evidence of physiologic dysfunction, (3) robust inflammatory response, (4) alteration in the alveolar-capillary barrier and, (5) histologic evidence of tissue injury (Matute-Bello et al., 2011; Semler et al., 2020). Large animal models of ARDS induced via repeated bronchoalveolar lavage (Araos et al., 2016), oleic acid (Borges et al., 2019) or endotoxin infusion (Nieman et al., 1996), gastric acid aspiration (Meers et al., 2011a) and inhalation injury (Leiphrahpam et al., 2021) have been reported, with each model mimicking certain aspects of the human disease to varying degrees (Ballard-Croft et al., 2012). However, few of these models rely on multifactorial etiologies of acute lung injury to both sides of the alveolar-capillary interface (Tiba et al., 2021) and few have been comprehensively evaluated regarding clinical, radiographic and histopathologic features.

We hypothesized that dual-hit injury to the epithelium and endothelium of the lung in human-sized swine can recapitulate moderate to severe human ARDS clinically, radiographically and histopathologically. In line with NHLBI and ATS research priorities, the goal of this study was to identify a reproducible method for inducing ARDS over an appropriate time scale to allow studies of new therapeutics within the context of organ dysfunction, organ support and co-interventions available to human patients. Such a pre-clinical model is crucial to maximize the utilization of resources in clinical trials.

¹Department of Surgery, Columbia University Medical Center, New York, NY 10032, USA. ²Department of Biomedical Engineering, Columbia University, New York, NY 10032, USA. ³Department of Surgery, Mount Sinai Hospital, Chicago, IL 60608, USA. ⁴Vagelos College of Physicians and Surgeons, Columbia University Medical Center, New York, NY 10032, USA. ⁵Institute of Comparative Medicine, Columbia University Medical Center, New York, NY 10032, USA. ⁶Department of Radiology, Columbia University Medical Center, New York, NY 10032, USA. ⁷Department of Pathology, Columbia University Medical Center, New York, NY 10032, USA. ⁸Department of Thoracic Surgery, Vanderbilt University Medical Center, Nashville, TN 37232, USA. ⁹Department of Pediatrics, Columbia University Medical Center, New York, NY 10032, USA. ¹⁰Department of Medicine, Columbia University Medical Center, New York, NY 10032, USA.

*These authors contributed equally to this work

‡Author for correspondence (gordana@columbia.edu)

DOI: 10.1242/dmm.049603; S.R.K., 0000-0002-2179-6787; J.A.R., 0000-0003-3950-2860; M.R.P., 0000-0003-1759-1145; M.R.H., 0000-0001-5854-0761; P.C., 0000-0003-4023-4752; J.S.L., 0000-0002-9940-2610; C.B.R.-S., 0000-0002-8921-3445; C.C.M., 0000-0001-6844-209X; M.B., 0000-0003-4456-4484; N.V.D., 0000-0002-1801-4975; G.V.-N., 0000-0002-9382-1574

This is an Open Access article distributed under the terms of the Creative Commons Attribution License (<https://creativecommons.org/licenses/by/4.0>), which permits unrestricted use, distribution and reproduction in any medium provided that the original work is properly attributed.

Handling Editor: Eckhard Wolf

Received 14 April 2022; Accepted 10 August 2022

RESULTS

Oxygenation impairment and clinical progression

We induced ARDS in the Yorkshire breed of swine by injuring the lungs of these animals with gastric acid and through infusion of endotoxin. For this, swine ($n=9$) were anesthetized, intubated and mechanically ventilated. Dual-hit injury induction was achieved by bronchoscopic delivery of standardized gastric contents (pH 2) followed by intravenous infusion of *Escherichia coli*-derived lipopolysaccharide. When the ratio of arterial oxygen partial pressure (PaO_2 in mm Hg) to fractional inspired oxygen (F_iO_2) had decreased to <150 – hereafter referred to ARDS 0 h – swine received standard ARDS treatment for up to 48 h. All swine developed moderate to severe ARDS (minimum $\text{PaO}_2:\text{F}_i\text{O}_2$ ratio of 80 ± 17). This produced a moderate to severe oxygenation impairment, i.e. a decrease in the ratio of arterial oxygen partial pressure (PaO_2 in mm Hg) to fractional inspired oxygen (F_iO_2) (minimum $\text{PaO}_2:\text{F}_i\text{O}_2$ ratio: 63–112), that failed to resolve (i.e. $\text{PaO}_2:\text{F}_i\text{O}_2>300$ on minimal ventilator settings) until at least 48 h after induction (see Fig. 1A, for experimental overview). Baseline measurements and characteristics of all animals were similar (Table S2). Following dual-hit injury induction, all nine animals met the diagnostic criteria for ARDS with an average minimal $\text{PaO}_2:\text{F}_i\text{O}_2$ ratio of 80 ± 17 . On arterial blood gas, the mean PaO_2 was significantly lower at ARDS 0 h (90.3 ± 27.2) relative to that at baseline (497.5 ± 38.3 , $P<0.001$). Of the nine animals, three

died prior to the planned study endpoint, i.e. at 2 h, 3 h or 8 h after onset of ARDS (ARDS 2 h, ARDS 3 h or ARDS 8 h, respectively) caused, respectively, by a massive pulmonary embolus, severe hypoxemia or a dislodged endotracheal tube, all resulting in hypoxic cardiopulmonary arrest. Although we observed variations between animals, the average time until ARDS 0 h – i.e. $\text{PaO}_2:\text{F}_i\text{O}_2<150$ following the completion of LPS infusion – was 1.5 ± 1.5 h (Table S3). The $\text{PaO}_2:\text{F}_i\text{O}_2$ ratio remained <300 , with minimal ventilator settings for ARDS 6 h endpoint animals ($n=3$) and ≤ 48 h. Owing to severely impaired oxygenation without improvement upon lung protective ventilation and/or paralytics, five animals required extracorporeal membrane oxygenation (ECMO).

ARDS induction was associated with arterial hypotension, pulmonary hypertension and respiratory acidosis. All animals developed arterial hypotension and seven out of nine animals required vasopressors to maintain a mean arterial blood pressure of >55 mm Hg. At ARDS 0 h, mean arterial pressure was below that of baseline (66 ± 8 mm Hg versus 80 ± 8 mm Hg) (Fig. 2), whereas pulmonary arterial pressure at ARDS 0 h was significantly elevated compared to baseline (47 ± 10 mm Hg versus 19 ± 5 mm Hg; $P<0.001$), primarily driven by hypoxemic and hypercapnic pulmonary vascular resistance, and minimally responsive to ventilator manipulation. Mean arterial pH at ARDS 0 h was significantly lower than mean arterial pH at baseline (7.318 ± 0.086 versus 7.455 ± 0.052 ; $P=0.002$) with an associated increase in PaCO_2

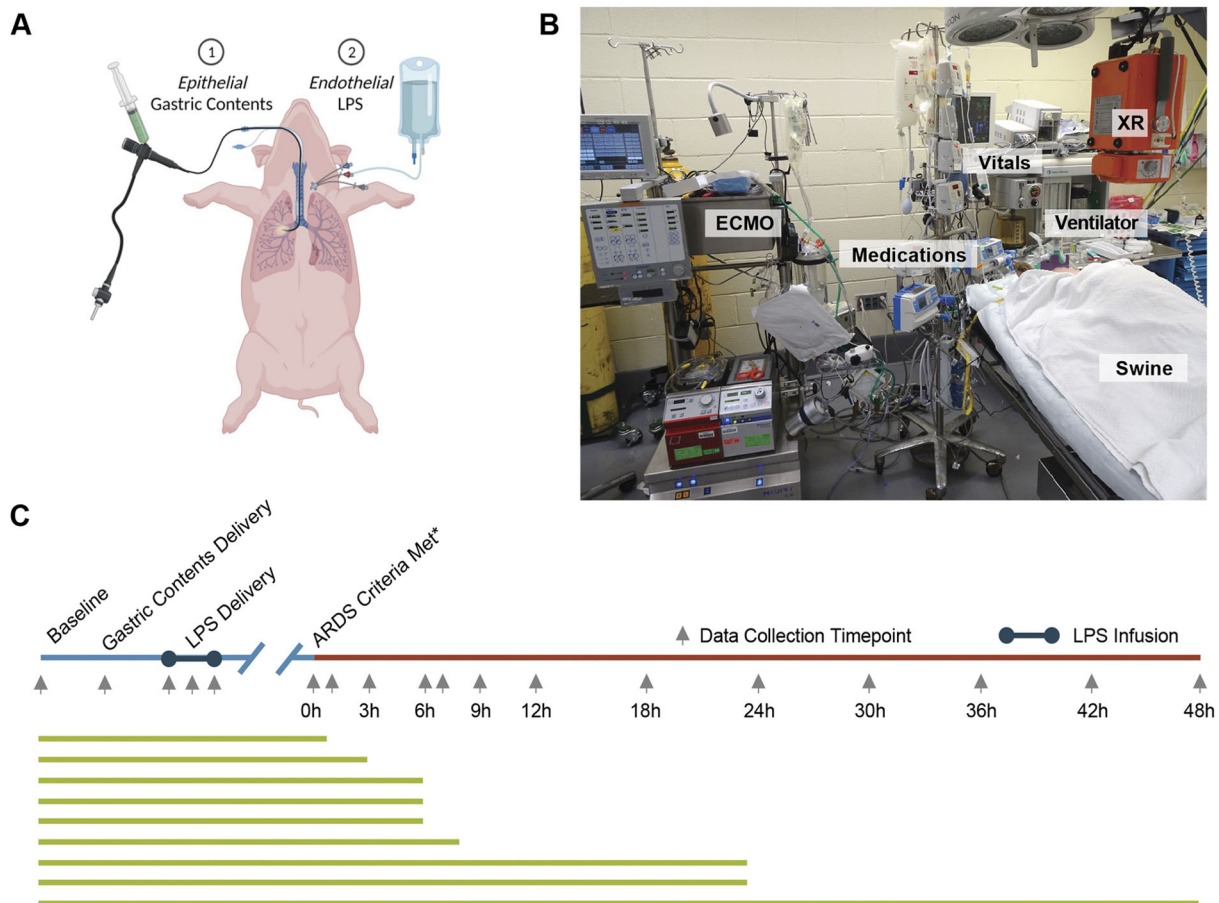


Fig. 1. Experimental overview. (A) Schematic of ARDS induction: epithelial lung injury induced by bronchoscopic delivery of 30–50 ml of standardized (pH 2.0) gastric contents to bilateral lungs, followed by central venous infusion of LPS. (B) Set-up of the operating room. (C) Data collection and experimental time course; green lines represent animal experiments. LPS, lipopolysaccharide; ABG, arterial blood gas; ECMO, extracorporeal membrane oxygenator; XR, X-ray machine.

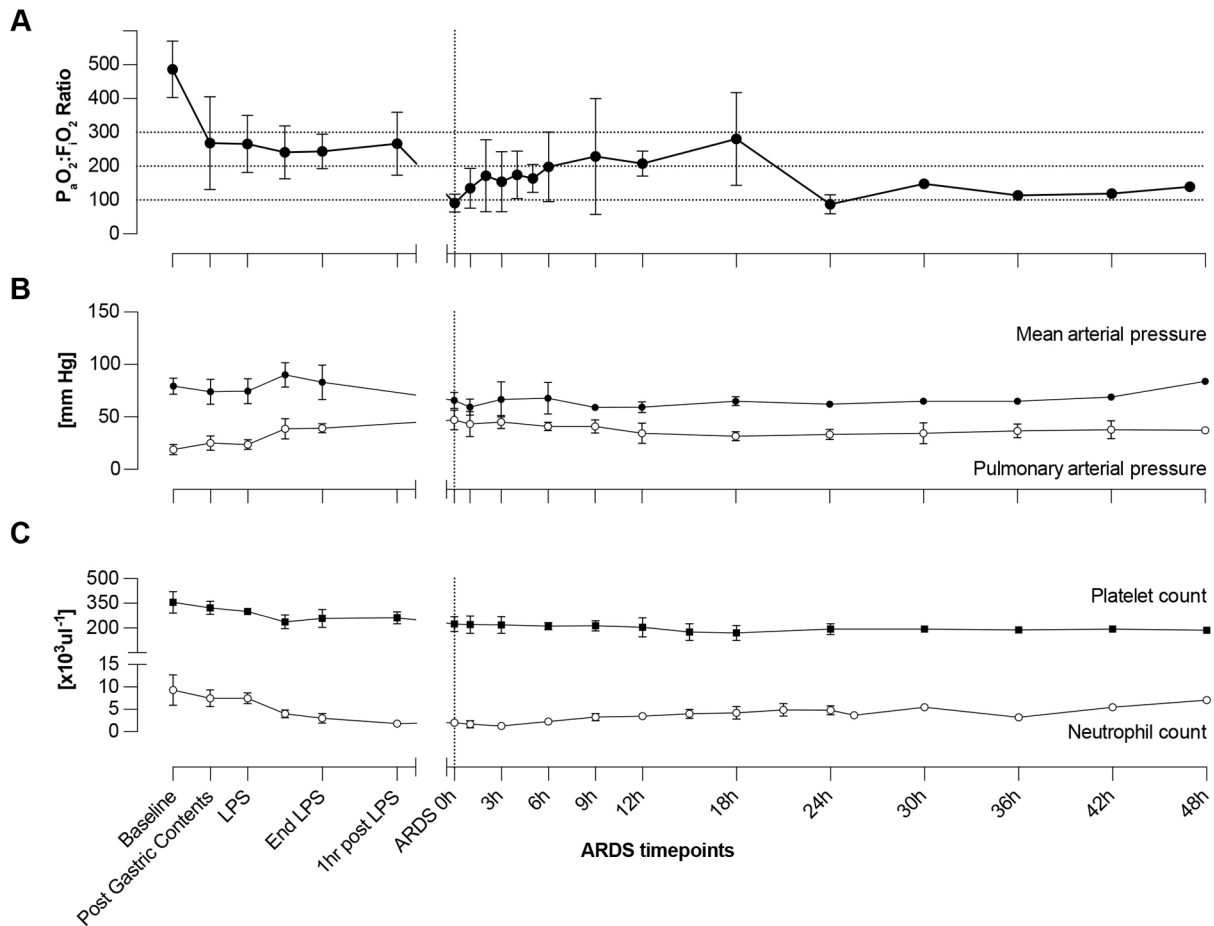


Fig. 2. Clinical measurements over experimental time course. (A) $P_{aO_2}:F_{iO_2}$ ratio as measured by arterial blood gas over experimental time course. (B) Mean arterial pressure (black) and pulmonary arterial pressures (open circles) in millimeters of mercury (mm Hg) over experimental time course. (C) Platelet (black circles) or neutrophil counts (open circles) [$\times 10^3 \mu\text{l}^{-1}$] over the experimental time course (in hours).

at ARDS 0 h (52 ± 7 versus 46 ± 5 ; $P=0.156$). Pulmonary arterial pressure remained elevated until the experimental endpoint (Fig. 2).

ARDS induction was also associated with a significant decline in the number of circulating neutrophils compared to those at baseline ($2.0 \pm 0.7 \times 10^3 \mu\text{l}^{-1}$ versus $9.3 \pm 3.4 \times 10^3 \mu\text{l}^{-1}$; $P=0.001$). In six out of eight animals, neutrophil counts reached a minimum between ARDS 0 h and ARDS 3 h (Fig. S2B, Fig. S3B, Fig. S4B, Fig. S5B, Fig. S6B, Fig. S7B, Fig. S8B, Fig. S9B). On average, numbers of circulating platelets also decreased following ARDS induction compared to those at baseline ($179 \pm 70 \times 10^3 \mu\text{l}^{-1}$ versus $356 \pm 66 \times 10^3 \mu\text{l}^{-1}$).

Plasma cytokines were measured in duplicate at baseline and ARDS 0 h. At ARDS 0 h, levels of pro-inflammatory cytokines, i.e. interleukins IL1A, IL2, IL6, IL12 and IL18 (hereafter referred to as IL-1 α , IL-2, IL-6, IL-12, IL-18, respectively) and tumor necrosis factor alpha (TNF- α) were significantly elevated relative to baseline (Fig. 3A). Additionally, concentrations of IL1B (hereafter referred to as IL-1 β) and its receptor antagonist IL1RN (also known as IL-1RA) were significantly increased at ARDS 0 h (134 – 1527 pg ml $^{-1}$, $P=0.038$ and 770 – $166,323$ pg ml $^{-1}$, $P=0.024$). Plasma concentration of the pro-inflammatory chemoattractant IL-8 was significantly elevated (249 – 7839 pg ml $^{-1}$). Levels of anti-inflammatory cytokines (IL-4 and IL-10) were also significantly increased at ARDS 0 h (36 – 4711 pg ml $^{-1}$, $P=0.0234$ and 294 – 4164 pg ml $^{-1}$; $P=0.0017$). Only levels of interferon

gamma (INFG; hereafter referred to as IFN- γ) were not significantly increased.

Acute-phase reactants (C-reactive protein, D-dimer, ferritin) were measured in blood plasma or serum by using ELISA (Table S5). Levels of D-dimer were significantly increased at ARDS 0 h in all animals ($P=0.004$) (Fig. 3B). Although not significant when compared as an average, C-reactive protein was elevated from baseline in all but one animal (Fig. 3B).

Radiographic evidence of lung edema

Interval chest X-rays demonstrated progressive bilateral opacification of the lung fields, consistent with the radiographic component of the Berlin criteria for ARDS diagnosis (Table S1, Fig. 4) (ARDS Definition Task Force et al., 2012). Semi-quantitative RALE scoring (as described in Warren et al., 2018) by two independent reviewers, interobserver agreement by Pearson's correlation coefficient ($r=0.88$, 95% CI 0.82–0.92, $P<0.001$; see Fig. S10A) and Bland-Altman plot (Fig. S10B) were high. Mean lung edema scores increased compared to baseline (11 ± 7) at ARDS 0 h (21 ± 7 , $P=0.005$; Fig. 4). Lung edema persisted after ARDS induction through endpoint and negatively correlated with the $P_{aO_2}:F_{iO_2}$ ratio ($P<0.001$). Lung edema was significantly worse in lower lung quadrants versus upper lung quadrants at ARDS 0 h (RALE score: 7.7 ± 2.1 versus 2.9 ± 2.8 , $P=0.016$) and 6 h (9.1 ± 2.0 versus 2.3 ± 2.0 , $P<0.001$) but not significantly different at

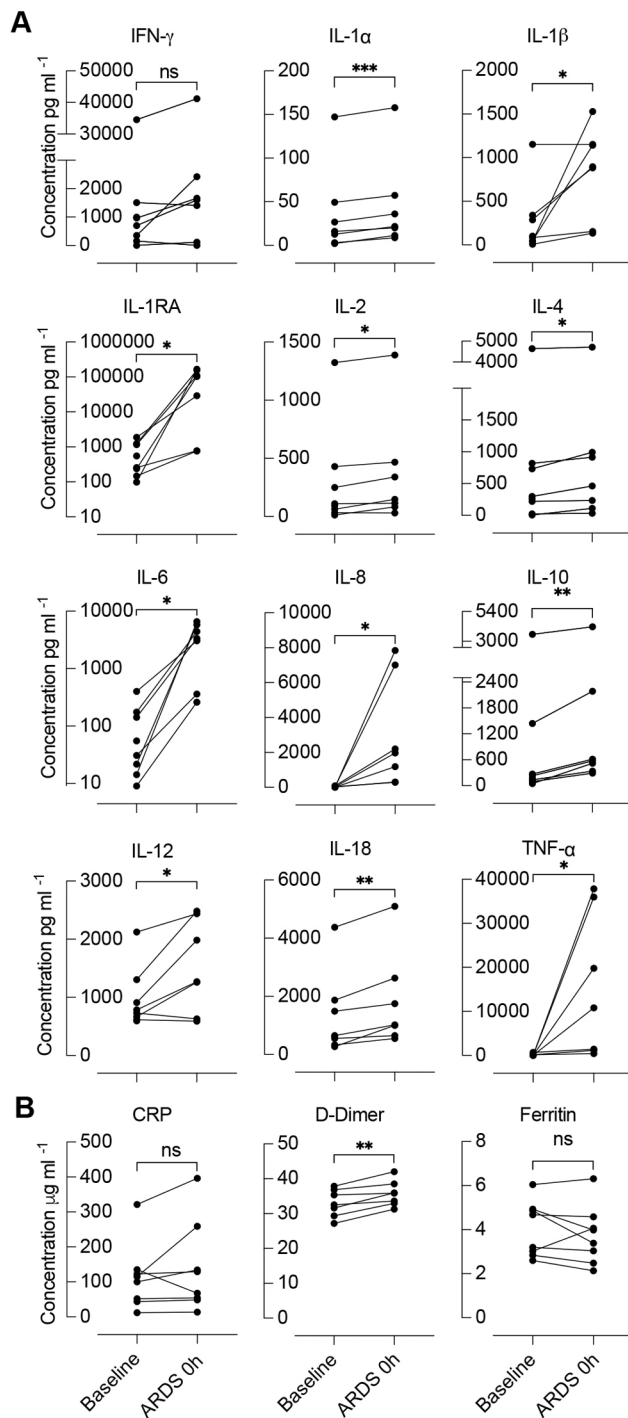


Fig. 3. Change in cytokine and acute-phase reactants from baseline to induction of ARDS. (A) Cytokine levels at baseline and ARDS 0 h ($n=7$). (B) Acute-phase reactants at baseline and ARDS 0 h ($n=7$). ns, not significant; * $P<0.05$; ** $P<0.01$; *** $P<0.001$. CRP, C-reactive protein. x-axis labeling shown in B also applies to all graphs in A.

ARDS 12 h (8.8 ± 3.0 versus 3.3 ± 2.5 , $P=0.114$) and ARDS 24 h (8.3 ± 0.4 versus 3.5 ± 2.5 , $P=0.254$) (Fig. 4; Fig. S11).

Histopathologic analysis

H&E slides of experimental and normal swine lung tissue were randomly numbered prior to pathologic review under light microscope by an experienced pulmonary pathologist. A

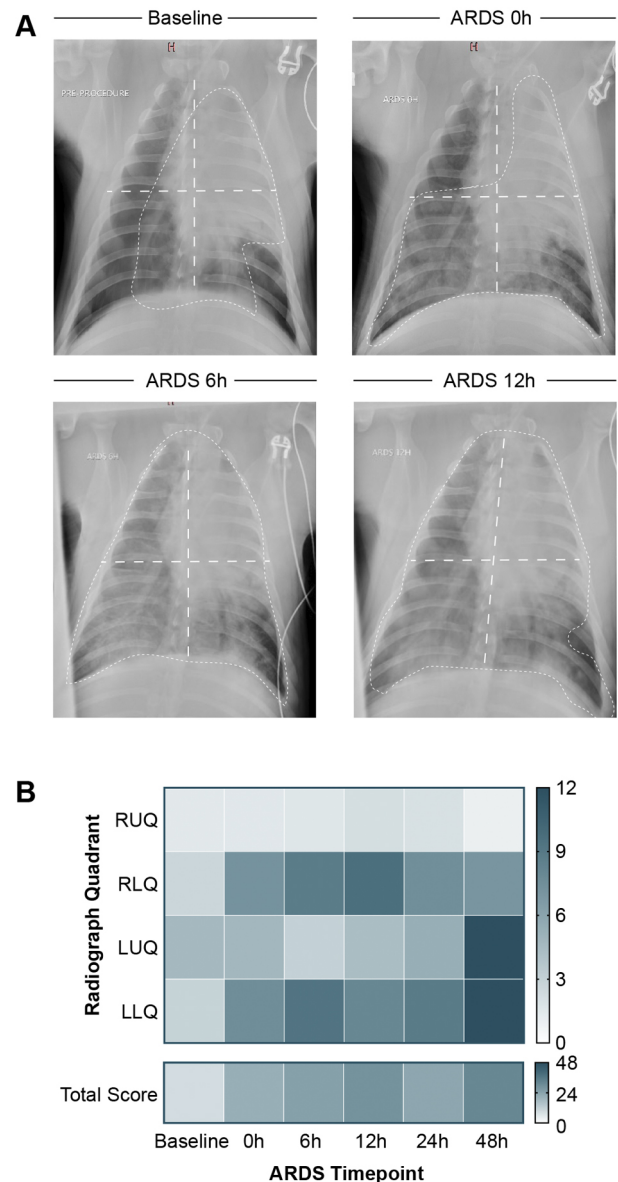


Fig. 4. Radiographic progression of ARDS. (A) Representative chest X-rays from baseline up to ARDS 12 h demonstrate radiographically the progression of ARDS (long dashed white lines, approximate delineation of lung field quadrants; short dashed white lines, area of radiographic edema). (B) Median radiographic assessment of lung edema score per radiographic lung field quadrant and as total for 'baseline' lung ($n=9$), ARDS 0 h ($n=7$), ARDS 6 h ($n=5$), ARDS 12 h ($n=3$), ARDS 24 h ($n=3$), ARDS 48 h ($n=1$). RUQ, right upper quadrant; RLQ, right lower quadrant; LUQ, left upper quadrant; LLQ, left lower quadrant. Color scale from white (0) to dark blue (12, individual lung field quadrant; 48, total score).

previously described lung-injury severity score, which includes the number of airway polymorphonuclear (PMN) cells per high-power field (hpf), the number of alveolar polymorphonuclear cells per hpf, alveolar edema, interstitial infiltrates (lymphocytes and neutrophils in the interstitium around vessels and airways and in alveolar septa and pleura) and interstitial edema (perivascular and peribronchial spaced expanded with edematous fluid), as described in O'Neill et al. (2017), was applied (Fig. S1D, Fig. S2E, Fig. S6E, Fig. S7E, Fig. S8E, Fig. S9E, Table S7). Minimal and maximum scores for each sub-score element are 0 and 3, respectively (except

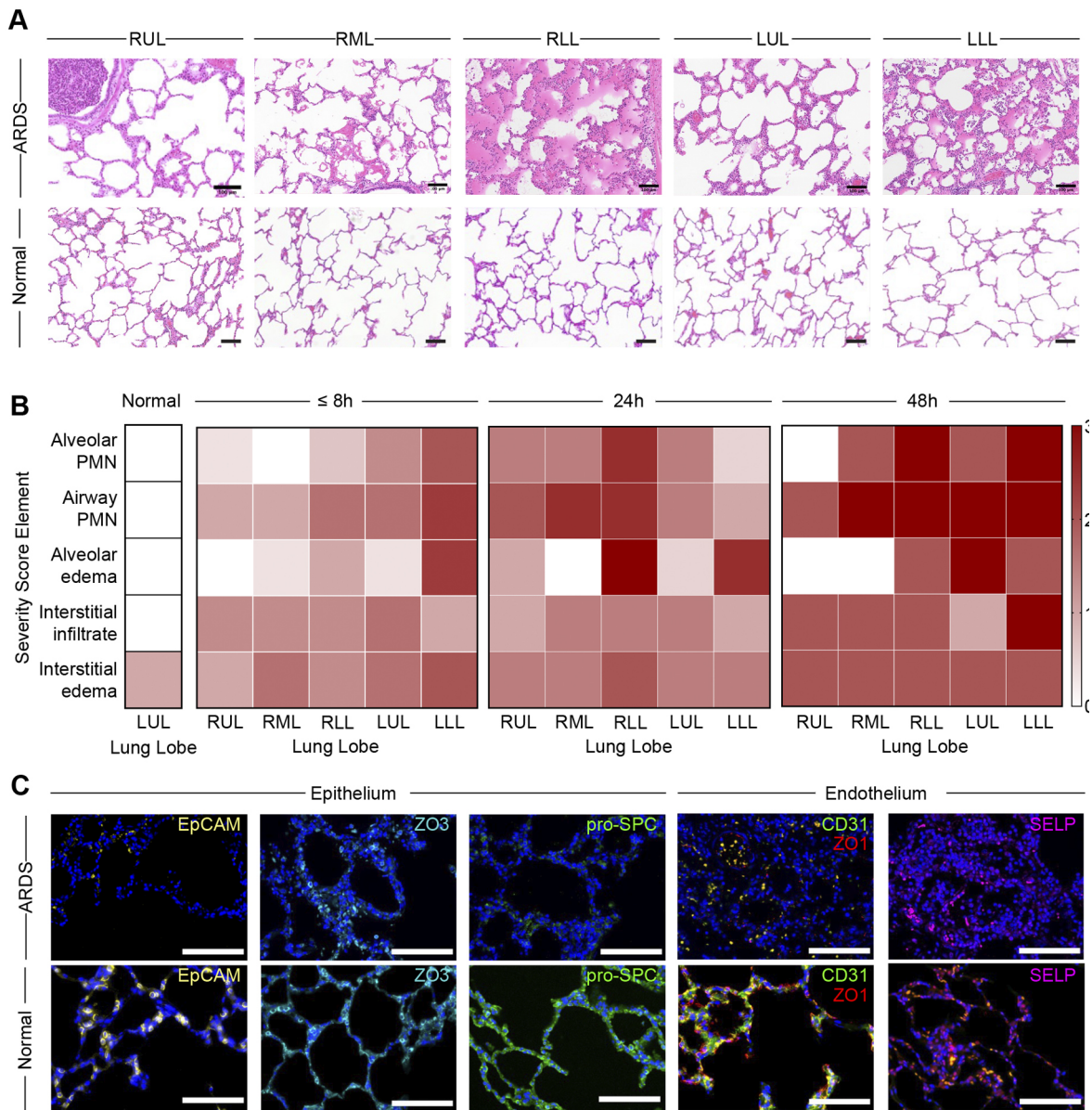


Fig. 5. Histopathologic analysis. (A) Representative H&E slides from ARDS and normal swine lungs arranged by lung lobe. (B) Lung injury severity score by severity score element and lung lobe by study endpoint (≤ 8 h, $n=3$; 24 h, $n=2$; 48 h, $n=1$). Color scale from white (normal) to red (severe injury). (C) Immunofluorescence images of ARDS and normal swine lungs stained for the epithelial markers EpCAM, ZO3 and pro-SPC, and the endothelial markers (CD31, ZO1 and SELP). RUL, right upper lobe; RML, right middle lobe; RLL, right lower lobe; LUL, left upper lobe; LLL, left lower lobe; PMN, polymorphonuclear cells. Scale bars: 100 μ m (A), 50 μ m (C).

interstitial edema, for which the maximum sub-score is 2). The average total lung injury severity score was 1.0 ± 0.0 for normal swine lungs, whereas the mean total lung injury severity score was 6.1 ± 1.8 at ARDS < 8 h, 7.7 ± 0.4 at ARDS 24 h, and 10.2 ± 2.8 at ARDS 48 h. Among score components, the interstitial edema and airway PMN sub-scores were highest for all experimental timepoints. Animals demonstrated time-dependent increases in interstitial edema (ARDS < 8 h: average 1.5 ± 0.1 ; ARDS 24 h: average 1.6 ± 0.3 ; ARDS 48 h: average 2.0 ± 0.0) and alveolar edema sub-scores (ARDS < 8 h: average 0.8 ± 0.7 ; ARDS 24 h: average 1.4 ± 0.0 ; 48 h: average 1.4 ± 1.3 , Fig. 5).

There was no significant difference in total lung injury severity score between left and right lower lobes (LLL and RLL, respectively) and non-lower lobes, i.e. right upper lobe (RUL), right middle lobe (RML) and left upper lobe (LUL) at ARDS < 8 h

($P=0.0838$), ARDS 24 h ($P=0.1361$), or ARDS 48 h ($P=0.1387$). However, lower lobes demonstrated higher alveolar edema sub-scores at ARDS < 8 h ($P=0.0103$) and ARDS 24 h ($P=0.0014$) but not at ARDS 48 h ($P=0.2191$). Hyaline membranes were not noted at study endpoint.

Immunofluorescence imaging showed decreased markers of both epithelial cell and endothelial cell adhesion [EpCAM and P-selectin (SELP), respectively] in lungs from animals with ARDS relative to those from healthy controls (Fig. 5C). Immunostaining for surfactant protein C (SFTPC; also known as pro-surfactant protein C, pro-SPC) a marker of type 2 alveolar epithelial cells (AT2), showed reduced immunofluorescence in lung tissue from ARDS swine compared to that in normal swine tissue. Markers of tight junctions and epithelial-endothelial barrier integrity (i.e. ZO3 and ZO1) were similarly decreased.

DISCUSSION

In this present study, we aimed to recapitulate the clinical, radiographic and histopathologic features of acute respiratory distress syndrome (ARDS) in a pre-clinical model to facilitate the study of potential therapeutics for this increasingly frequent and severe lung disease. We modeled the pathophysiology of ARDS by using two clinically relevant injuries (gastric acid aspiration and endotoxin infusion) and fulfilled the criteria delineated by the NHLBI and ATS for representative ARDS model (Matute-Bello et al., 2011). We addressed the critical gap in the need for pre-clinical models that can be used to deepen our understanding of the pathophysiology of ARDS, identify biomarkers of each phase of disease and test emerging targeted therapies.

ARDS induction by gastric acid injury and endotoxin reliably produced moderate to severe oxygenation impairment that failed to resolve up to 48 h after induction, suggesting that the lung injury is not merely a transient pneumonitis. Rapid onset after the inciting event is a key pre-model feature. One recently published swine model utilizing both direct and indirect lung injury reached a PaO_2 : FiO_2 ratio of ≤ 300 by ARDS 12 h; however, the mean PaO_2 : FiO_2 ratio was above the threshold for severe ARDS (Tiba et al., 2021). The induction timeframe in that model (i.e. with PaO_2 : FiO_2 ratios consistent with moderate to severe ARDS within 1.5 ± 1.5 h following infusion of LPS) mimics the clinical progression of ARDS in humans and aligns with the temporal diagnostic criterion of ARDS (ARDS Definition Task Force et al., 2012). In one large single-institution study, human patients with early-onset ARDS developed ARDS within 4.2 h, the interquartile range being 2.3–7.4 (Fuchs et al., 2019).

We also observed strong evidence of physiologic dysfunction beyond oxygen impairment. All hemodynamic responses and changes in laboratory values seen after intravenous infusion of LPS (i.e. leukopenia, decreased cardiac output and arterial hypotension) (Matute-Bello et al., 2008) were observed, as were significant increases in pulmonary arterial pressure. Because the model of ARDS presented here involves human-sized animals, measurement and monitoring of these parameters within an intensive-care-unit level of care is possible, circumventing the practical difficulties of repeated blood sampling and prolonged organ support that limit the applicability of small animal models. To confirm the alterations in the inflammatory response are consistent with ARDS, glucocorticoids were not administered (Meduri et al., 1995). Furthermore, interventions, such as prone positioning, vasopressors, crystalloid fluid administration, neuromuscular blockade and ECMO, were co-administered in a manner consistent with that provided to humans. An advantage of this model is the ability to test candidate treatments in a clinical context, thereby mimicking that of human patients.

Neutrophils are central mediators of the pathogenesis of acute lung injury and crucial for the robust inflammatory response of ARDS (Abraham et al., 2000; Folkesson et al., 1995). Excessive neutrophil recruitment to the lungs and neutrophil activation contribute to the progression of ARDS through damage of bystander tissue and further loss of lung function (Grommes and Soehnlein, 2011; Williams and Chambers, 2014). Our finding that levels of circulating neutrophils significantly decrease (69–93%) between ARDS 0 h and ARDS 6 h (Fig. 2C) suggests that neutrophils are largely sequestered within the pulmonary vasculature, parenchyma and airways. We found that accumulation of neutrophils within the alveoli and airways in lung tissues worsened over the experimental time course (Fig. 5), i.e. at

all three histopathologic analysis timepoints after ARDS 0 h lung tissue contained on average >300 PMN cells per hpf compared to 22 PMNs per hpf in control lung specimens. Additionally, levels of IL-8 – a potent neutrophil chemoattractant (Grommes and Soehnlein, 2011; Williams and Chambers, 2014) and suggested biomarker for ARDS (Whitney et al., 2020; Yadav et al., 2018) – were significantly elevated from baseline at ARDS 0 h in our experimental model (Fig. 3).

Other elements of the inflammatory response also developed after dual-hit lung injury. As previously demonstrated in patients with ARDS, levels of pro-inflammatory cytokines in the experimental animals were significantly elevated at ARDS 0 h relative to those at baseline (Fig. 3) (Meduri et al., 1995; Puneet et al., 2005; Schütte et al., 1996). Plasma concentrations of IL-1 β and its receptor antagonist IL-1RA, both of which were significantly elevated after ARDS induction in our model, correlated with ARDS severity and have been associated with clinical outcomes (Meduri et al., 1995).

Alteration of the alveolar-capillary barrier and development of alveolar edema are key pathophysiologic features of ARDS. Two independent reviewers semi-quantitatively analyzed lung edema by chest radiography, and found that mean lung edema had increased from baseline to ARDS 0 h, correlating with worsening oxygenation (Fig. 4). This alteration of the alveolar-capillary barrier was further demonstrated by histopathologic analysis. Diffuse alveolar injury – i.e. the near pathologic correlate to the clinical entity of ARDS – involves the accumulation of neutrophils in alveolar or interstitial spaces, formation of hyaline membranes, thickening of the alveolar wall and enhanced injury (Cardinal-Fernandez et al., 2017; Matute-Bello et al., 2011). In our study, we did not observe hyaline membranes in most swine. But Cardinal-Fernandez et al. also found hyaline membranes and diffuse alveolar damage (DAD) in only half of human patients undergoing open-lung biopsies for clinical ARDS (Cardinal-Fernandez et al., 2017). The predominant lack of hyaline membranes in the swine model might relate to the timescale of our study or the peripheral location of the lung specimens. Other pathologic features of the acute exudative phase of ARDS (i.e. of diffuse alveolar damage, interstitial and alveolar edema, inflammation, and fibrin deposition) were observed with increasing severity of lung injury over the experimental time course (Fig. 5).

Other swine models have examined alternative injury-induction methods, i.e. repeated saline lavage together with ventilation injury (Araos et al., 2021, 2016), volutrauma and hyperoxia followed by direct inoculation of *Escherichia coli* by acidified gastric particles (Tiba et al., 2021). Most ARDS animal models have demonstrated injury to the lung epithelium or changes in the pulmonary vascular compartment, including hypertension and the formation of microthrombi (Araos et al., 2016; Borges et al., 2019; Nieman et al., 1996; Meers et al., 2011a; Leiphrakpam et al., 2021), but few have demonstrated alterations to both sides of the alveolar-capillary interface in a manner consistent with ARDS in human patients (Millar et al., 2020). The sheep model used by Millar and colleagues enables the mechanistic study of ARDS pathophysiology and is highly suitable for developing and evaluating therapeutics because it recapitulates the clinicopathologic features of injury to both the epithelium and endothelium in ARDS.

Ex vivo models, in which human lungs were injured by intrabronchial instillation of endotoxin (Lee et al., 2009), have also been used for pre-clinical testing of candidate therapies (Shaw et al., 2019). One pre-clinical model specifically evaluated permeability of the lung endothelial barrier and clearance of the

alveolar fluid, and treatment with bone marrow-derived multipotent mesenchymal stem cells (MSCs) (Lee et al., 2009; Millar et al., 2020) and informed subsequent clinical trials in humans (Matthay et al., 2019). This phase 2a safety trial demonstrated the safety of allogeneic MSCs for patients with moderate to severe ARDS but did not evaluate its efficacy (Matthay et al., 2019). Because the swine model presented here comprehensively recapitulates ARDS within a clinically relevant context beyond the endothelial barrier, it is particularly well suited to evaluate dosing strategies and pre-clinical efficacy of candidate therapeutics, such as MSCs or their secretome, to maximize resources dedicated to clinical trials.

Limitations

Variations in mechanism and intensity of lung injury may provide insights into the pathophysiologic mechanisms of ARDS (Beitler et al., 2022). Although acid aspiration is a reproducible mechanism of lung injury, the window between injurious and non-injurious doses is narrow (Matute-Bello et al., 2008), making tuning of the degree of injury and ARDS severity difficult. The animal-to-animal variability of this model accurately captures inter-patient variability but cannot detect small variations in biomarkers or clinical data. By their very nature, experimental models emulate simplified and tightly controlled clinical scenarios, a limitation that also applies to our study. We investigated the inflammatory response in the lungs to bronchoalveolar lavage. Our model was designed to mimic the clinical course and treatments experienced by human patients. However, due to the severe lung dysfunction that occurred by establishing the ARDS conditions in our model, we were unable to reliably perform bronchoscopy without compromising oxygenation and recruitment of the lungs. Furthermore, swine commonly have underlying lung disease and bacterial colonization, which may augment the severity of ARDS in this model.

Our model is resource intensive, requiring around-the-clock intensive care by trained medical and veterinary doctors. Additionally, the model allows for co-interventions (e.g. ECMO), which might not be available to all patients in all clinical settings, as it requires specialized equipment and staffing. Furthermore, a follow-up period of 48 h is a very short clinical timeframe in the context of the lengthy pathology of ARDS, particularly as it evolves over the course of weeks. Future studies focusing on the efficacy of novel therapeutics would require an extended experimental time course.

Conclusion

This pre-clinical model in human-sized swine recapitulates the clinical, radiographic, and histopathologic manifestations of ARDS, providing a much-needed tool to study pathogenesis and targeted therapeutics for this highly morbid, and increasingly incident, lung disease.

MATERIALS AND METHODS

Additional details regarding materials and methods are provided in the Supplementary Materials and Methods as indicated. All animals were treated in accordance with the Guide for the Care and Use of Laboratory Animals, 8th Edition and housed in facilities accredited by the Association for Assessment and Accreditation of Laboratory Animal Care International (AAALACI). All studies were approved by the Institutional Animal Care and Use Committee of Columbia University (National Research Council, 2011).

Pre-procedure preparation

Female Yorkshire swine (49±5 kg, Table S2) were placed under intravenous general anesthesia after sedation with tiletamine/zolazepam. They were initially ventilated by using volume-control with tidal volume (V_T) 10–12 ml kg⁻¹, positive end-expiratory pressure (PEEP) of 5 cm H₂O,

respiratory rate (RR) at 12–20 breaths min⁻¹ and fraction of inspired oxygen ($F_{I}O_2$) of 100%.

ARDS induction

Gastric aspiration injury was induced by positioning a bronchoscope tip into bilateral mainstem bronchi to deliver 30–50 ml standardized gastric contents (pH 2) (Fraisie et al., 2007; Guenthart et al., 2019; Meers et al., 2011b). Lipopolysaccharide (LPS) from *Escherichia coli* O55:B5 was then infused centrally for 30–60 min (see Fig. 1A for experimental overview).

ARDS 0 h was defined as the time when the $PaO_2:F_{I}O_2$ ratio first decreased to <150 mm Hg following LPS infusion. At ARDS 0 h, lung-protective ventilation was initiated (V_T 6 ml kg⁻¹, PEEP and $F_{I}O_2$ per ARDSNet ‘Higher $F_{I}O_2$ ’ parameters) (Table S4); the RR was titrated to maintain pH>7.3. PEEP and $F_{I}O_2$ were gradually removed as tolerated, depending on pulse oximetry and PaO_2 . The muscle relaxant pancuronium bromide was used to paralyze animals with severe hypoxia and/or hypercarbia. Swine were moved into prone position every 6–12 h when able to tolerate position changes. ECMO was used as rescue therapy to prevent mortality prior to planned endpoint.

Data and sample collection

Blood samples and chest radiographs were taken at pre-defined timepoints (Fig. 1). Experimental endpoints were ARDS 6 h ($n=3$) and ARDS 48 h. Animals were euthanized prior to planned experimental endpoint when their clinical status deteriorated despite maximal medical treatment, including vasopressor support, ECMO and/or attempted cardiopulmonary resuscitation. Inflammatory markers, i.e. interferon gamma (IFN- γ), interleukins (IL-1 α , IL-1 β , IL-2, IL-4, IL-6, IL-8, IL-10, IL-12, IL-18, interleukin receptor antagonist (IL1RN; also known as IL-1RA) and tumor necrosis factor (TNF; also known as TNF- α) were analyzed in duplicate by using the Porcine Cytokine 13-Plex Discovery Assay (Eve Technologies, Calgary, AB, Canada). Other markers, i.e. D-dimer, C-reactive protein (CRP) and ferritin, were measured by using commercially available enzyme-linked immunosorbent assays (ELISAs) according to the manufacturer’s instructions (Table S5).

Radiographic assessment of lung edema (RALE) scoring

Radiographs were blinded for evaluation of lung edema using the RALE score by two radiologists. Each radiologist independently scored the radiographs to evaluate the extent of consolidation and density of alveolar opacities (Table S6) (Warren et al., 2018).

Histopathologic analysis of lung injury

Lung tissue samples were fixed, paraffin-embedded and sectioned. Hematoxylin and Eosin (H&E)-stained slides were reviewed blinded by a pulmonary pathologist using a previously described lung injury severity score (Table S7) (Guenthart et al., 2019). The pathologist was provided with background information regarding the study aims but slides were completely masked as to experimental group or timepoint, as described by Meyerholz and Beck (2018). Lung sections were stained for additional proteins and cell markers, i.e. for epithelial cell adhesion molecule (EPCAM), tight junction protein 1 (TJP1; also known as zonula occludens-1, ZO1), tight junction protein ZO-3 (TJP3, also known as zonula occludens-1, ZO3), surfactant protein C (SFTPC; also known as pro-surfactant protein C, pro-SPC), platelet and endothelial cell adhesion molecule 1 (PECAM1; also known as CD31) and P-selectin (SELP) (see Table S8 for antibody information).

Statistical analysis

One-way analysis of variance with Tukey’s multiple comparison post hoc tests and Student’s *t*-tests were performed using Prism Version 9 (GraphPad). A value of $P<0.05$ was considered statistically significant.

Acknowledgements

The authors thank Dominik Hajosi, Alicia McLuckie, Melissa Tamimi and Bryan Lui for their assistance in the care of animals; Alexander Romanov for his coordination of animal experiments; and Kenmond Fung and Hermogenes Lopez for their support in maintaining animals on ECMO.

Competing interests

The authors declare no competing or financial interests.

Author contributions

Conceptualization: S.R.K., J.A.R., M.R.P., M.G.M., M.L.K., M.B., N.V.D., G.V.-N.; Methodology: S.R.K., J.A.R., M.R.P., M.R.H., P.C., M.G.M., M.L.K., J.S.L., C.B.R.-S., C.C.M., M.B., N.V.D., G.V.-N.; Formal analysis: S.R.K., J.A.R., M.R.P., M.R.H., P.C., M.G.M., M.L.K., J.S.L., C.B.R.-S., C.C.M., M.B., N.V.D., G.V.-N.; Investigation: S.R.K., J.A.R., M.R.P., M.R.H., P.C., M.G.M., M.L.K.; Resources: N.V.D., G.V.-N.; Data curation: S.R.K., J.A.R., M.R.P., M.R.H., P.C., M.G.M., M.L.K., G.V.-N.; Writing - original draft: S.R.K., J.A.R., M.R.P., M.G.M., M.L.K., J.S.L., C.B.R.-S., C.C.M., M.B., N.V.D., G.V.-N.; Writing - review & editing: S.R.K., J.A.R., M.R.P., M.R.H., P.C., M.G.M., M.L.K., J.S.L., C.B.R.-S., C.C.M., M.B., N.V.D., G.V.-N.; Visualization: S.R.K., J.A.R., N.V.D.; Supervision: N.V.D., G.V.-N.; Project administration: S.R.K., J.A.R., N.V.D., G.V.-N.; Funding acquisition: N.V.D., G.V.-N.

Funding

The authors gratefully acknowledge funding support of this research provided by the National Institutes of Health (5T32 HL007854, P41 EB027062, 2R01 HL120046 and U01HL134760). Open Access funding provided by Irving Medical Center, Columbia University. Deposited in PMC for immediate release.

References

- Abraham, E., Carmody, A., Shenkar, R. and Arcaroli, J. (2000). Neutrophils as early immunologic effectors in hemorrhage- or endotoxemia-induced acute lung injury. *Am. J. Physiol. Lung Cell. Mol. Physiol.* **279**, L1137-L1145. doi:10.1152/ajplung.2000.279.6.L1137
- Acute Respiratory Distress Syndrome Network, Brower, R. G., Matthay, M. A., Morris, A., Schoenfeld, D., Thompson, B. T. and Wheeler, A. (2000). Ventilation with lower tidal volumes as compared with traditional tidal volumes for acute lung injury and the acute respiratory distress syndrome. *N. Engl. J. Med.* **342**, 1301-1308. doi:10.1056/NEJM200005043421801
- Araos, J., Alegria, L., Garcia, P., Damiani, F., Tapia, P., Soto, D., Salomon, T., Rodriguez, F., Amthauer, M., Erranz, B. et al. (2016). Extracorporeal membrane oxygenation improves survival in a novel 24-h pig model of severe acute respiratory distress syndrome. *Am. J. Transl. Res.* **8**, 2826-2837.
- Araos, J., Alegria, L., Garcia, A., Cruces, P., Soto, D., Erranz, B., Salomon, T., Medina, T., Garcia, P., Dubo, S. et al. (2021). Effect of positive end-expiratory pressure on lung injury and haemodynamics during experimental acute respiratory distress syndrome treated with extracorporeal membrane oxygenation and near-apnoeic ventilation. *Br. J. Anaesth.* **127**, 807-814. doi:10.1016/j.bja.2021.07.031
- ARDS Definition Task Force, Ranieri, V. M., Rubenfeld, G. D., Thompson, B. T., Ferguson, N. D., Caldwell, E., Fan, E., Camporota, L. and Slutsky, A. S. (2012). Acute respiratory distress syndrome: the Berlin definition. *JAMA* **307**, 2526-2533. doi:10.1001/jama.2012.5669
- Ballard-Croft, C., Wang, D., Sumpter, L. R., Zhou, X. and Zwischenberger, J. B. (2012). Large-animal models of acute respiratory distress syndrome. *Ann. Thorac. Surg.* **93**, 1331-1339. doi:10.1016/j.athoracsurg.2011.06.107
- Beitler, J. R., Thompson, B. T., Baron, R. M., Bastarache, J. A., Denlinger, L. C., Esserman, L., Gong, M. N., LaVange, L. M., Lewis, R. J., Marshall, J. C. et al. (2022). Advancing precision medicine for acute respiratory distress syndrome. *Lancet Respir. Med.* **10**, 107-120. doi:10.1016/S2213-2600(21)00157-0
- Bellani, G., Laffey, J. G., Pham, T., Fan, E., Brochard, L., Esteban, A., Gattinoni, L., van Haren, F., Larsson, A., McAuley, D. F. et al. (2016). Epidemiology, patterns of care, and mortality for patients with acute respiratory distress syndrome in intensive care units in 50 countries. *JAMA* **315**, 788-800. doi:10.1001/jama.2016.0291
- Borges, A. M., Ferrari, R. S., Thomaz, L., Ulbrich, J. M., Félix, E. A., Silvello, D. and Andrade, C. F. (2019). Challenges and perspectives in porcine model of acute lung injury using oleic acid. *Pulm. Pharmacol. Ther.* **59**, 101837. doi:10.1016/j.pupt.2019.101837
- Cardinal-Fernandez, P., Lorente, J. A., Ballén-Barragán, A. and Matute-Bello, G. (2017). Acute respiratory distress syndrome and diffuse alveolar damage: new insights on a complex relationship. *Ann. Am. Thorac. Soc.* **14**, 844-850. doi:10.1513/AnnalsATS.201609-728PS
- Combes, A., Hajage, D., Capellier, G., Demoule, A., Lavoue, S., Guervilly, C., Da Silva, D., Zafrani, L., Tirot, P., Veber, B. et al. (2018). Extracorporeal membrane oxygenation for severe acute respiratory distress syndrome. *N. Engl. J. Med.* **378**, 1965-1975. doi:10.1056/NEJMoa1800385
- Folkesson, H. G., Matthay, M. A., Hébert, C. A. and Broaddus, V. C. (1995). Acid aspiration-induced lung injury in rabbits is mediated by interleukin-8-dependent mechanisms. *J. Clin. Invest.* **96**, 107-116. doi:10.1172/JCI118009
- Fraisse, A., Bregeon, F., Delpierre, S., Gaudart, J., Payan, M. J., Pugin, J. and Papazian, L. (2007). Hemodynamics in experimental gastric juice induced aspiration pneumonia. *Intensive Care Med.* **33**, 300-307. doi:10.1007/s00134-006-0457-2
- Fuchs, L., Feng, M., Novack, V., Lee, J., Taylor, J., Scott, D., Howell, M., Celi, L. and Talmor, D. (2019). The effect of ARDS on survival: do patients die from ARDS or with ARDS? *J. Intensive Care Med.* **34**, 374-382. doi:10.1177/0885066617717659
- Grommes, J. and Soehnlein, O. (2011). Contribution of neutrophils to acute lung injury. *Mol. Med.* **17**, 293-307. doi:10.2119/molmed.2010.00138
- Guenthart, B. A., O'Neill, J. D., Kim, J., Queen, D., Chicotka, S., Fung, K., Simpson, M., Donocoff, R., Salna, M., Marboe, C. C. et al. (2019). Regeneration of severely damaged lungs using an interventional cross-circulation platform. *Nat. Commun.* **10**, 1985. doi:10.1038/s41467-019-09908-1
- Lee, J. W., Fang, X., Gupta, N., Serikov, V. and Matthay, M. A. (2009). Allogeneic human mesenchymal stem cells for treatment of E. coli endotoxin-induced acute lung injury in the ex vivo perfused human lung. *Proc. Natl. Acad. Sci. USA* **106**, 16357-16362. doi:10.1073/pnas.0907996106
- Leiphrakpam, P. D., Weber, H. R., McCain, A., Matas, R. R., Duarte, E. M. and Buesing, K. L. (2021). A novel large animal model of smoke inhalation-induced acute respiratory distress syndrome. *Respir. Res.* **22**, 198. doi:10.1186/s12931-021-01788-8
- Matthay, M. A., McAuley, D. F. and Ware, L. B. (2017). Clinical trials in acute respiratory distress syndrome: challenges and opportunities. *Lancet Respir. Med.* **5**, 524-534. doi:10.1016/S2213-2600(17)30188-1
- Matthay, M. A., Calfee, C. S., Zhuo, H., Thompson, B. T., Wilson, J. G., Levitt, J. E., Rogers, A. J., Gotts, J. E., Wiener-Kronish, J. P., Bajwa, E. K. et al. (2019). Treatment with allogeneic mesenchymal stromal cells for moderate to severe acute respiratory distress syndrome (START study): a randomised phase 2a safety trial. *Lancet Respir. Med.* **7**, 154-162. doi:10.1016/S2213-2600(18)30418-1
- Matute-Bello, G., Frevert, C. W. and Martin, T. R. (2008). Animal models of acute lung injury. *Am. J. Physiol. Lung Cell. Mol. Physiol.* **295**, L379-L399. doi:10.1152/ajplung.00010.2008
- Matute-Bello, G., Downey, G., Moore, B. B., Groshong, S. D., Matthay, M. A., Slutsky, A. S. and Kuebler, W. M. and Acute Lung Injury in Animals Study Group. (2011). An official American Thoracic Society workshop report: features and measurements of experimental acute lung injury in animals. *Am. J. Respir. Cell Mol. Biol.* **44**, 725-738. doi:10.1165/rcmb.2009-0210ST
- Meduri, G. U., Headley, S., Kohler, G., Stentz, F., Tolley, E., Umberger, R. and Leeper, K. (1995). Persistent elevation of inflammatory cytokines predicts a poor outcome in ARDS. Plasma IL-1 β and IL-6 levels are consistent and efficient predictors of outcome over time. *Chest* **107**, 1062-1073. doi:10.1378/chest.107.4.1062
- Meers, C. M., De Wever, W., Verbeken, E., Mertens, V., Wauters, S., De Vleeschauwer, S. I., Vos, R., Vanaudenaerde, B. M., Verleden, G. M. and Van Raemdonck, D. E. (2011a). A porcine model of acute lung injury by instillation of gastric fluid. *J. Surg. Res.* **166**, e195-e204. doi:10.1016/j.jss.2010.10.015
- Meers, C. M., Tsagkaropoulos, S., Wauters, S., Verbeken, E., Vanaudenaerde, B., Scheers, H., Verleden, G. M. and Van Raemdonck, D. (2011b). A model of ex vivo perfusion of porcine donor lungs injured by gastric aspiration: a step towards pretransplant preconditioning. *J. Surg. Res.* **170**, e159-e167. doi:10.1016/j.jss.2011.05.015
- Meyerholz, D. K. and Beck, A. P. (2018). Principles and approaches for reproducible scoring of tissue stains in research. *Lab. Invest.* **98**, 844-855. doi:10.1038/s41374-018-0057-0
- Millar, J. E., Bartnikowski, N., Passmore, M. R., Obonyo, N. G., Malfetherneier, M. V., von Bahr, V., Redd, M. A., See Hoe, L., Ki, K. K., Pedersen, S. et al. (2020). Combined mesenchymal stromal cell therapy and extracorporeal membrane oxygenation in acute respiratory distress syndrome. A randomized controlled trial in sheep. *Am. J. Respir. Crit. Care Med.* **202**, 383-392. doi:10.1164/rccm.201911-2143OC
- National Research Council. (2011). *Guide for the Care and Use of Laboratory Animals*, 8th edn. Washington, DC: The National Academies Press.
- Nieman, G. F., Gatto, L. A., Paskanik, A. M., Yang, B., Fluck, R. and Picone, A. (1996). Surfactant replacement in the treatment of sepsis-induced adult respiratory distress syndrome in pigs. *Crit. Care Med.* **24**, 1025-1033. doi:10.1097/00003246-199606000-00024
- O'Neill, J., Guenthart, B., Kim, J., Chicotka, S., Queen, D., Fung, K., Marboe, C., Romanov, A., Huang, S. X. L., Chen, Y.-W. et al. (2017). Cross-circulation for extracorporeal support and recovery of the lung. *Nat. Biomed. Eng.* **1**, 0037. doi:10.1038/s41551-017-0037
- Papazian, L., Forel, J. M., Gacouin, A., Penot-Ragon, C., Perrin, G., Loundou, A., Jaber, S., Arnal, J. M., Perez, D., Seghboyan, J. M. et al. (2010). Neuromuscular blockers in early acute respiratory distress syndrome. *N. Engl. J. Med.* **363**, 1107-1116. doi:10.1056/NEJMoa1005372
- Peek, G. J., Mugford, M., Tiruvoipati, R., Wilson, A., Allen, E., Thalanany, M. M., Hibbert, C. L., Truesdale, A., Clemens, F., Cooper, N. et al. (2009). Efficacy and economic assessment of conventional ventilatory support versus extracorporeal membrane oxygenation for severe adult respiratory failure (CESAR): a multicentre randomised controlled trial. *Lancet* **374**, 1351-1363. doi:10.1016/S0140-6736(09)61069-2

- Puneet, P., Mochhala, S. and Bhatia, M.** (2005). Chemokines in acute respiratory distress syndrome. *Am. J. Physiol. Lung Cell. Mol. Physiol.* **288**, L3-L15. doi:10.1152/ajplung.00405.2003
- Schütte, H., Lohmeyer, J., Rosseau, S., Ziegler, S., Siebert, C., Kielisch, H., Pralle, H., Grimminger, F., Morr, H. and Seeger, W.** (1996). Bronchoalveolar and systemic cytokine profiles in patients with ARDS, severe pneumonia and cardiogenic pulmonary oedema. *Eur. Respir. J.* **9**, 1858-1867. doi:10.1183/09031936.96.09091858
- Semler, M. W., Bernard, G. R., Aaron, S. D., Angus, D. C., Biros, M. H., Brower, R. G., Calfee, C. S., Colantuoni, E. A., Ferguson, N. D., Gong, M. N. et al.** (2020). Identifying clinical research priorities in adult pulmonary and critical care. NHLBI working group report. *Am. J. Respir. Crit. Care Med.* **202**, 511-523. doi:10.1164/rccm.201908-1595WS
- Shaw, T. D., McAuley, D. F. and O'Kane, C. M.** (2019). Emerging drugs for treating the acute respiratory distress syndrome. *Expert Opin Emerg. Drugs* **24**, 29-41. doi:10.1080/14728214.2019.1591369
- Tiba, M. H., McCracken, B. M., Leander, D. C., Colmenero, C. I., Nemzek, J. A., Sjoding, M. W., Konopka, K. E., Flott, T. L., VanEpps, J. S., Daniels, R. C. et al.** (2021). A novel swine model of the acute respiratory distress syndrome using clinically relevant injury exposures. *Physiol. Rep.* **9**, e14871. doi:10.14814/phy2.14871
- Warren, M. A., Zhao, Z., Koyama, T., Bastarache, J. A., Shaver, C. M., Semler, M. W., Rice, T. W., Matthay, M. A., Calfee, C. S. and Ware, L. B.** (2018). Severity scoring of lung oedema on the chest radiograph is associated with clinical outcomes in ARDS. *Thorax* **73**, 840-846. doi:10.1136/thoraxjnl-2017-211280
- Whitney, J. E., Zhang, B., Koterba, N., Chen, F., Bush, J., Graham, K., Lacey, S. F., Melenhorst, J. J., Teachey, D. T., Mensinger, J. L. et al.** (2020). Systemic endothelial activation is associated with early acute respiratory distress syndrome in children with extrapulmonary sepsis. *Crit. Care Med.* **48**, 344-352. doi:10.1097/CCM.0000000000004091
- Williams, A. E. and Chambers, R. C.** (2014). The mercurial nature of neutrophils: still an enigma in ARDS? *Am. J. Physiol. Lung Cell. Mol. Physiol.* **306**, L217-L230. doi:10.1152/ajplung.00311.2013
- Yadav, H., Bartley, A., Keating, S., Meade, L. A., Norris, P. J., Carter, R. E., Gajic, O. and Kor, D. J.** (2018). Evolution of validated biomarkers and intraoperative parameters in the development of postoperative ARDS. *Respir. Care* **63**, 1331-1340. doi:10.4187/respcare.06103

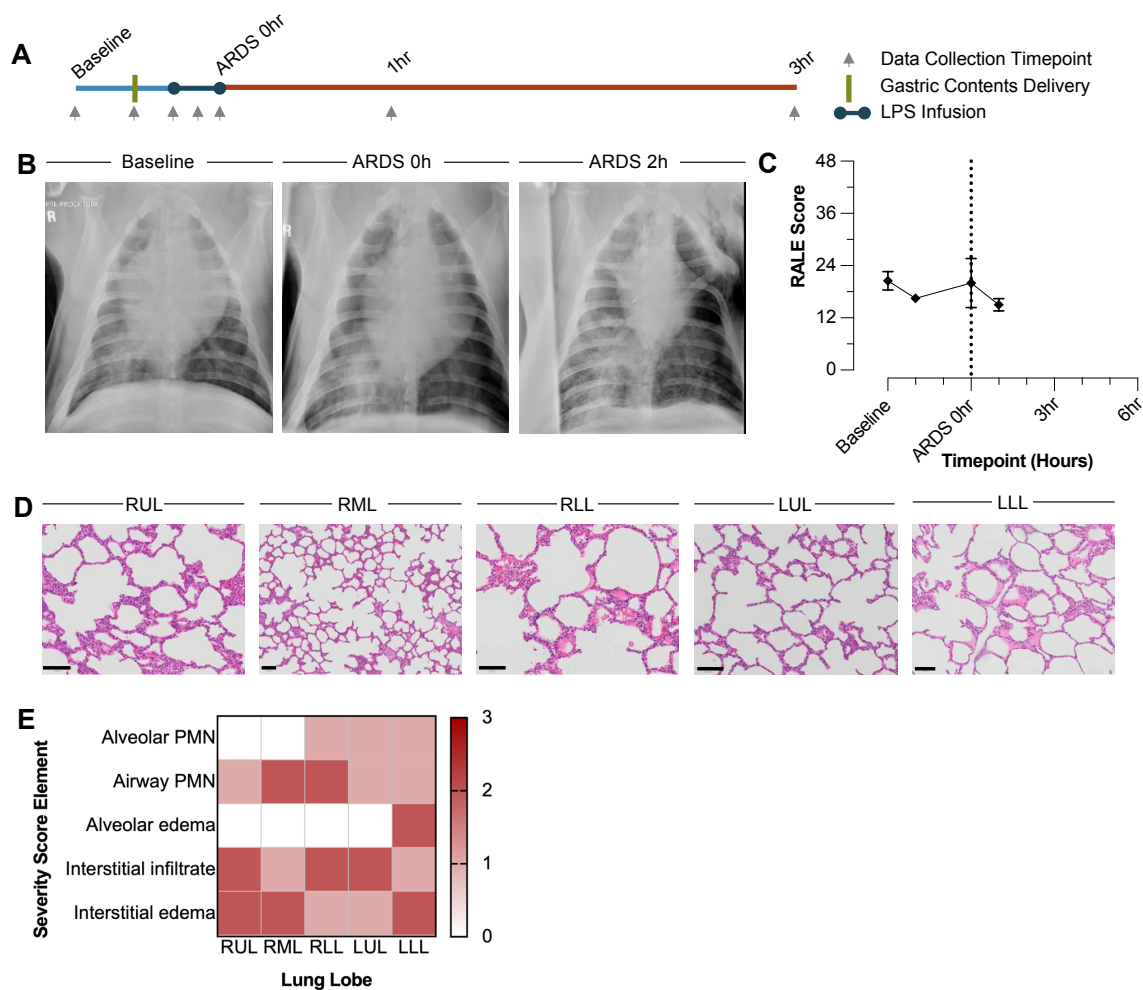


Fig. S1. ARDS 1 - 54411. (A) Experimental timecourse. (B) Chest radiographs at baseline, ARDS 0hr, and ARDS 2hr. (C) Radioagraphic Assessment of Lung Edema scores. (D) H&E section from lung tissue at study endpoint. Scale bar = 100 μ m. (E) Heatmap of lung injury severity score by score element and lung lobe. GC = gastric contents, LPS = lipopolysaccharide, RALE = Radiographic Assessment of Lung Edema, RUL = right upper lobe, RML = right middle lobe, RLL = right lower lobe, LUL = left upper lobe, LLL = left lower lobe.

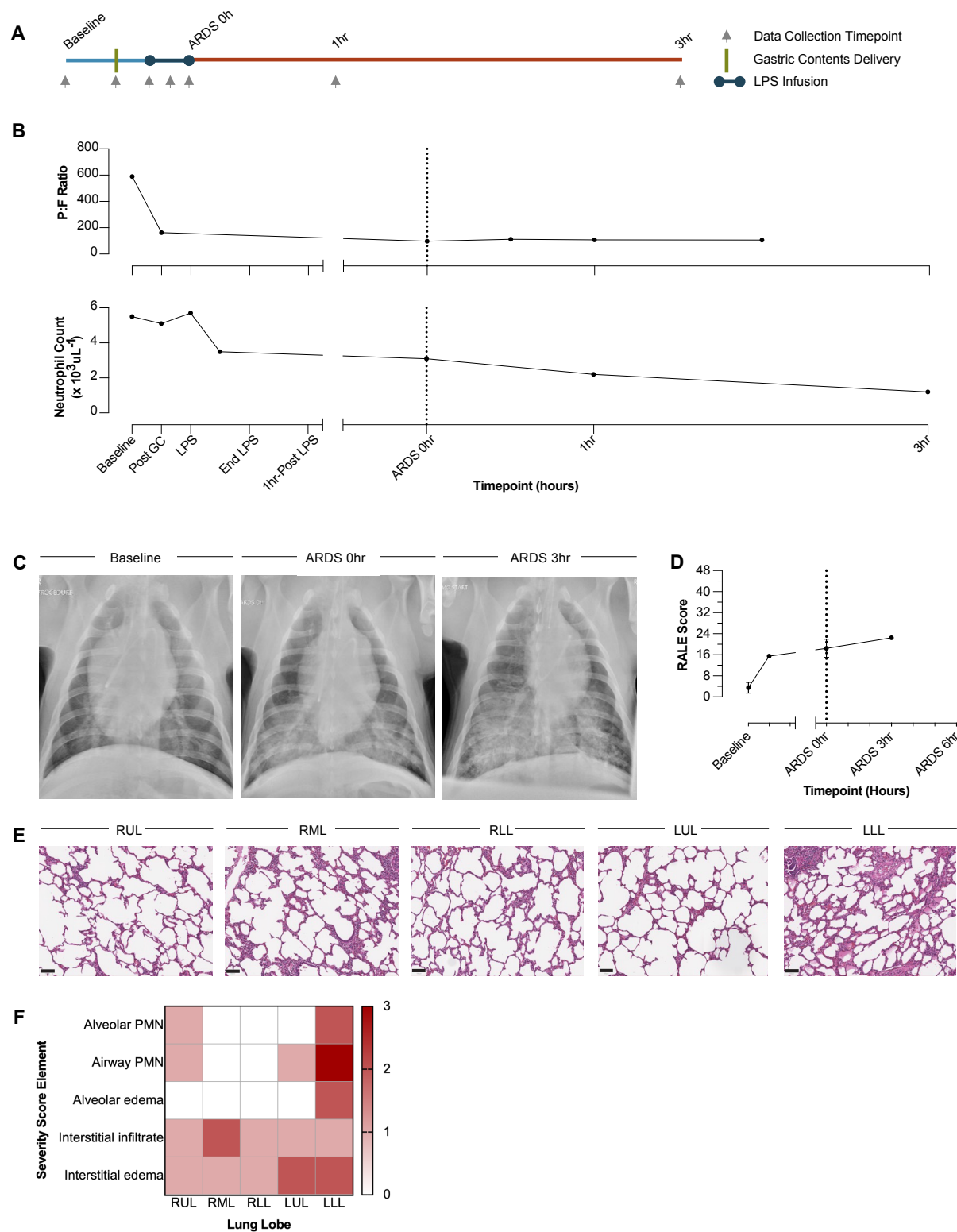


Fig. S2. ARDS 9 - 55369. (A) Experimental timecourse. (B) $\text{PaO}_2\text{:FI}_2\text{O}_2$ ratio over experimental timecourse; neutrophil count ($\times 10^3 \mu\text{L}^{-1}$). (C) Chest radiographs at baseline, ARDS 0hr, and ARDS 3hr. (D) Radiographic Assessment of Lung Edema scores. (E) H&E section from lung tissue at study endpoint. Scale bar = 100 μm . (F) Heatmap of lung injury severity score by score element and lung lobe. GC = gastric contents, LPS = lipopolysaccharide, RALE = Radiographic Assessment of Lung Edema, RUL = right upper lobe, RML = right middle lobe, RLL = right lower lobe, LUL = left upper lobe, LLL = left lower lobe.

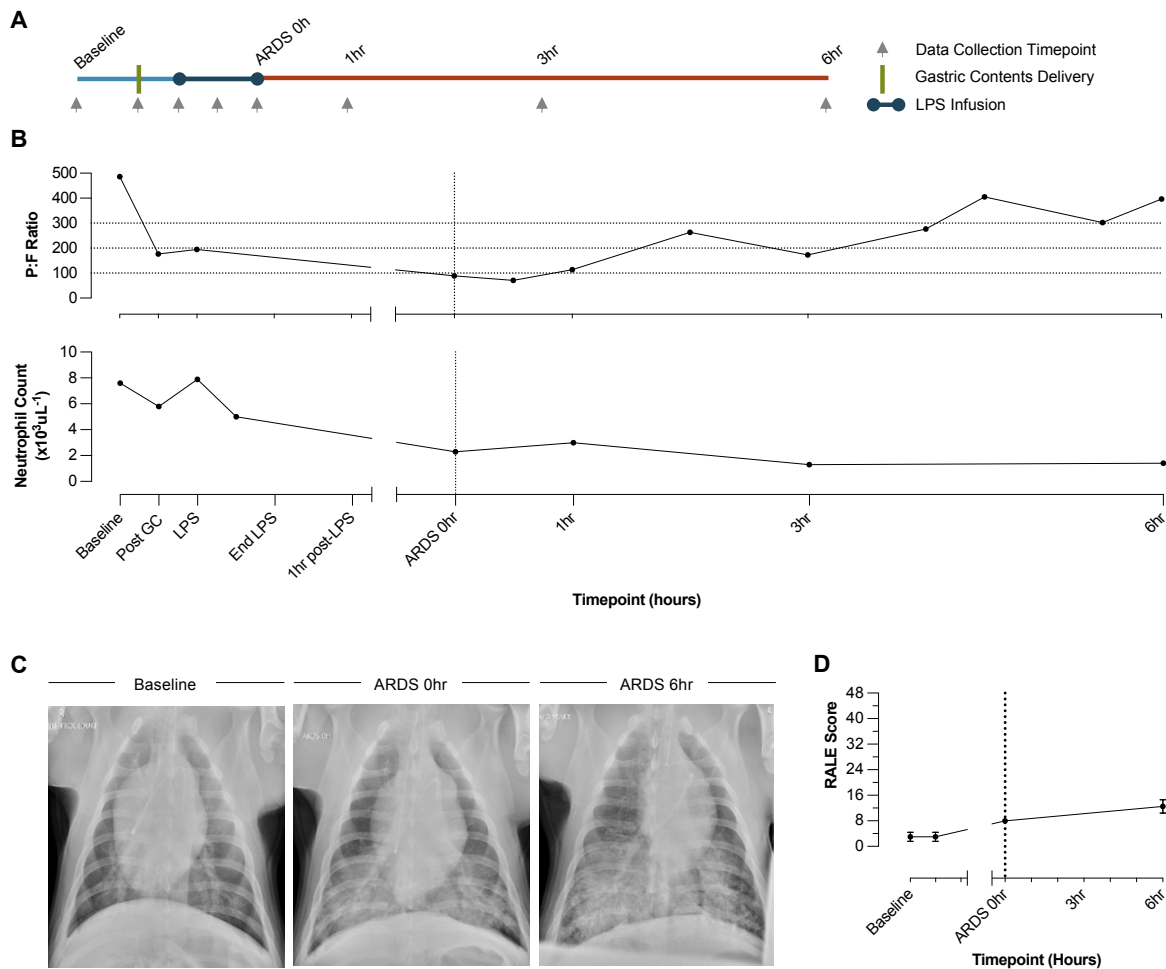


Fig. S3. ARDS 6 - 54990. (A) Experimental timecourse. (B) $P_aO_2:F_iO_2$ ratio over experimental timecourse; neutrophil count ($\times 10^3 \mu L^{-1}$). (C) Chest radiographs at baseline, ARDS 0hr, and ARDS 6hr. (D) Radioagraphic Assessment of Lung Edema scores. GC = gastric contents, LPS = lipopolysaccharide, RALE = Radiographic Assessment of Lung Edema, RUL = right upper lobe, RML = right middle lobe, RLL = right lower lobe, LUL = left upper lobe, LLL = left lower lobe.

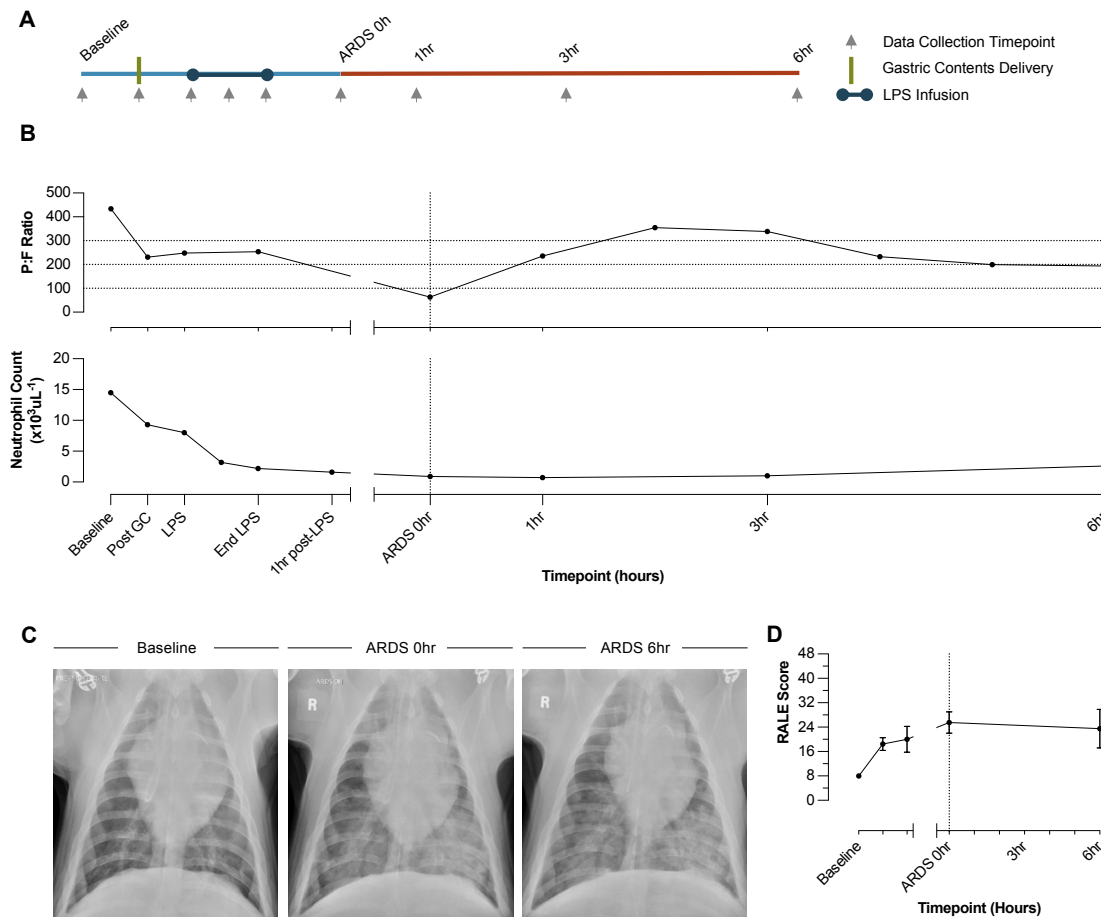


Fig. S4. ARDS 8 - 55214. (A) Experimental timecourse. (B) Pa_{O2}:Fi_{O2} ratio over experimental timecourse; neutrophil count (x10³μL⁻¹). (C) Chest radiographs at baseline, ARDS 0hr, and ARDS 6hr. (D) Radioagraphic Assessment of Lung Edema scores. GC = gastric contents, LPS = lipopolysaccharide, RALE = Radiographic Assessment of Lung Edema, RUL = right upper lobe, RML = right middle lobe, RLL = right lower lobe, LUL = left upper lobe, LLL = left lower lobe.

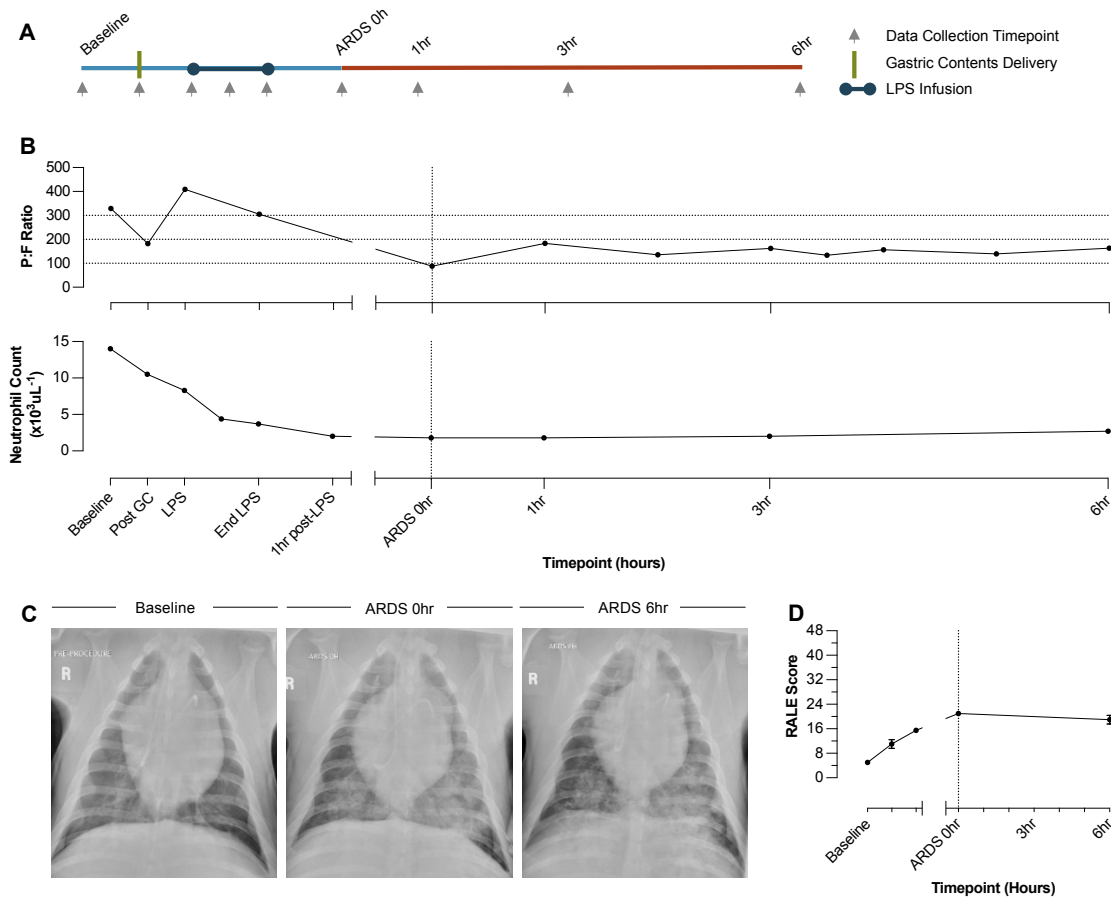


Fig. S5. ARDS 10 - 55368. (A) Experimental timecourse. (B) Pa_{O2}:FI_{O2} ratio over experimental timecourse; neutrophil count (x10³μL⁻¹). (C) Chest radiographs at baseline, ARDS 0hr, and ARDS 6hr. (D) Radioagraphic Assessment of Lung Edema scores. GC = gastric contents, LPS = lipopolysaccharide, RALE = Radiographic Assessment of Lung Edema, RUL = right upper lobe, RML = right middle lobe, RLL = right lower lobe, LUL = left upper lobe, LLL = left lower lobe.

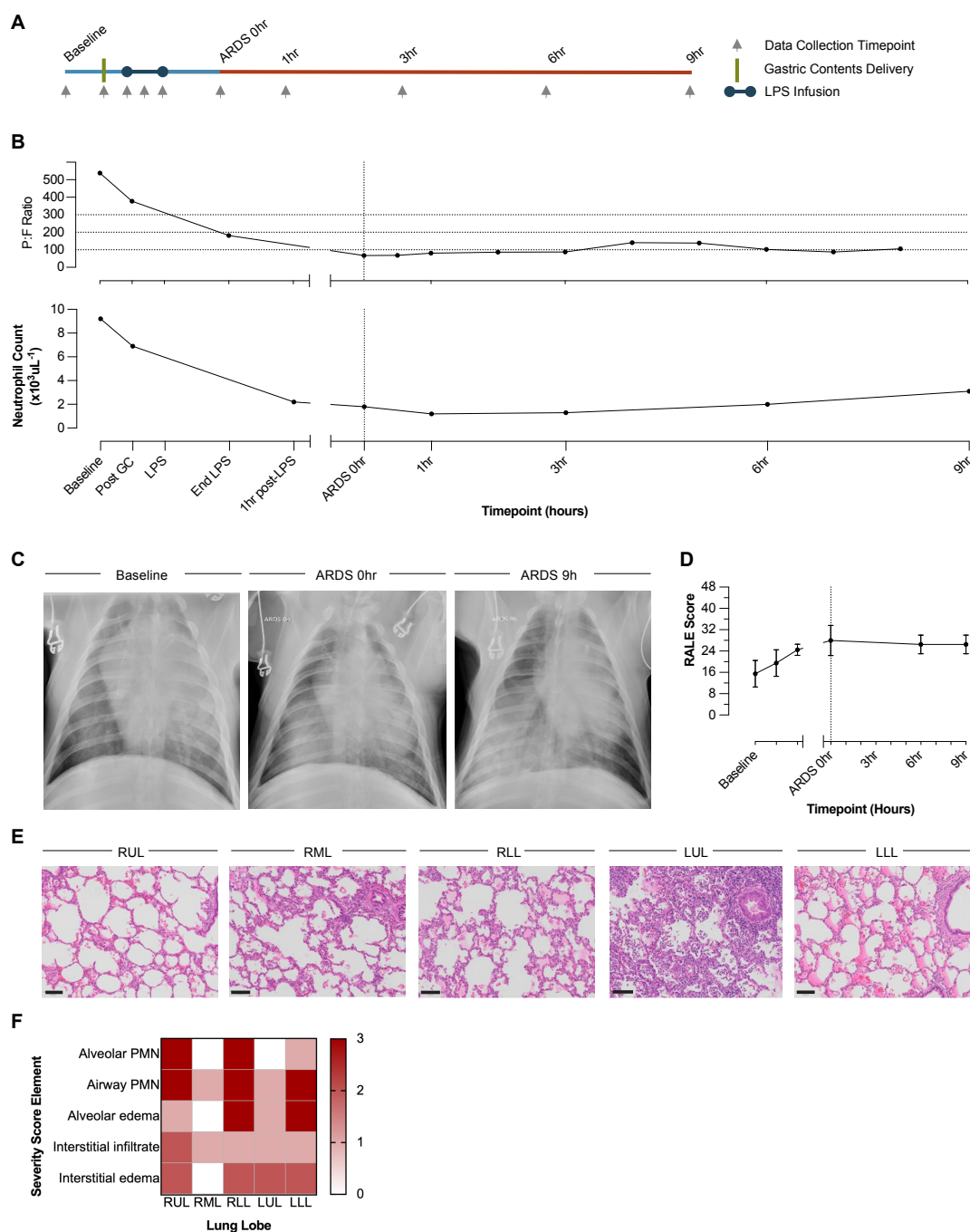


Fig. S6. ARDS 3 - 54633. (A) Experimental timecourse. (B) $\text{Pa}_{\text{O}_2}:\text{Fi}_{\text{O}_2}$ ratio over experimental timecourse; neutrophil count ($\times 10^3 \mu\text{L}^{-1}$). (C) Chest radiographs at baseline, ARDS 0hr, and ARDS 9hr. (D) Radiographic Assessment of Lung Edema scores. (E) H&E section from lung tissue at study endpoint. Scale bar = 100 μm . (F) Heatmap of lung injury severity score by score element and lung lobe. GC = gastric contents, LPS = lipopolysaccharide, RALE = Radiographic Assessment of Lung Edema, RUL = right upper lobe, RML = right middle lobe, RLL = right lower lobe, LUL = left upper lobe, LLL = left lower lobe.

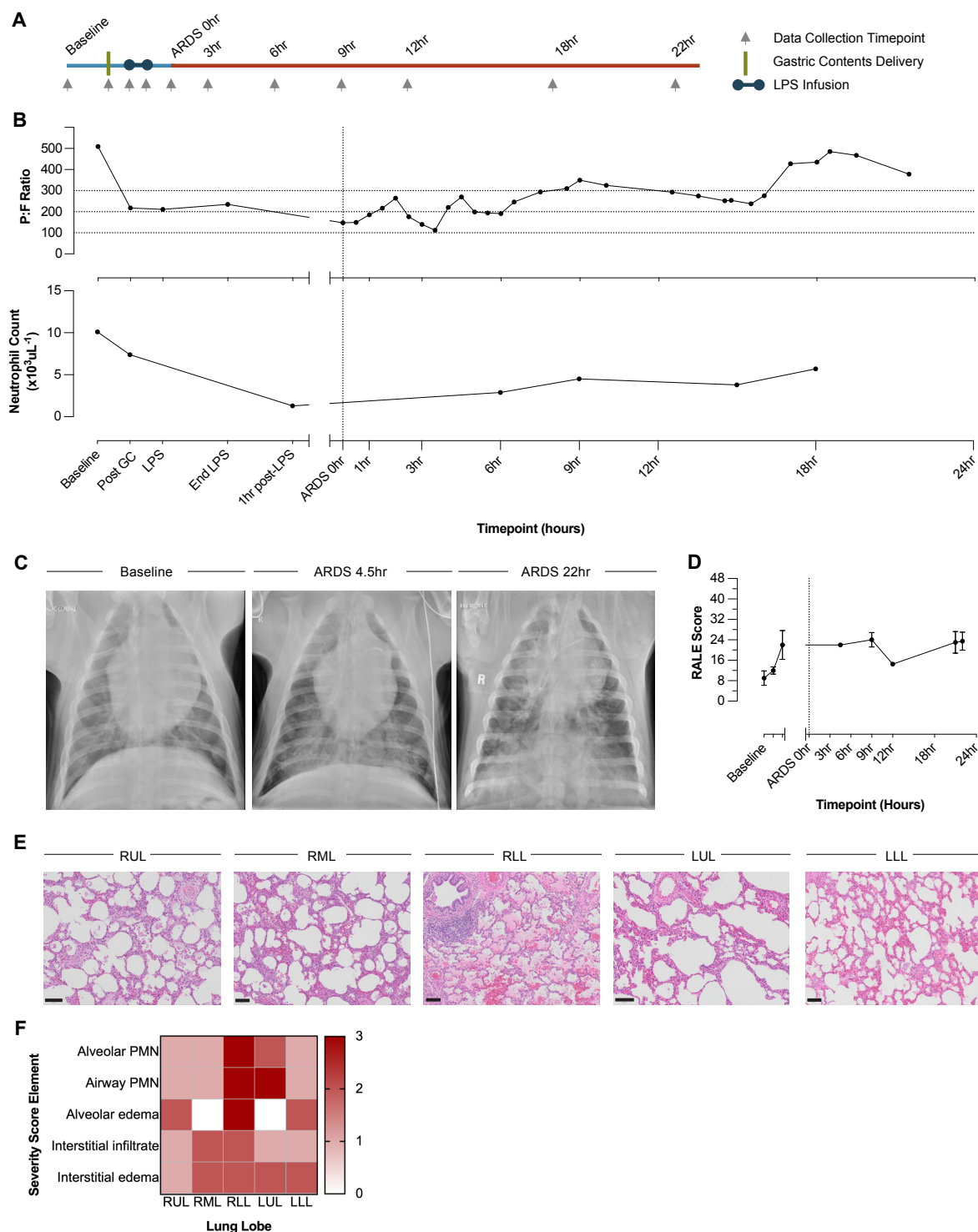


Fig. S7. ARDS 7 - 55146. (A) Experimental timecourse. (B) $\text{PaO}_2:\text{FIO}_2$ ratio over experimental timecourse; neutrophil count ($\times 10^3 \mu\text{L}^{-1}$). (C) Chest radiographs at baseline, ARDS 4.5hr, and ARDS 22hr. (D) Radiographic Assessment of Lung Edema scores. (E) H&E section from lung tissue at study endpoint. Scale bar = 100 μm . (F) Heatmap of lung injury severity score by score element and lung lobe. GC = gastric contents, LPS = lipopolysaccharide, RALE = Radiographic Assessment of Lung Edema, RUL = right upper lobe, RML = right middle lobe, RLL = right lower lobe, LUL = left upper lobe, LLL = left lower lobe.

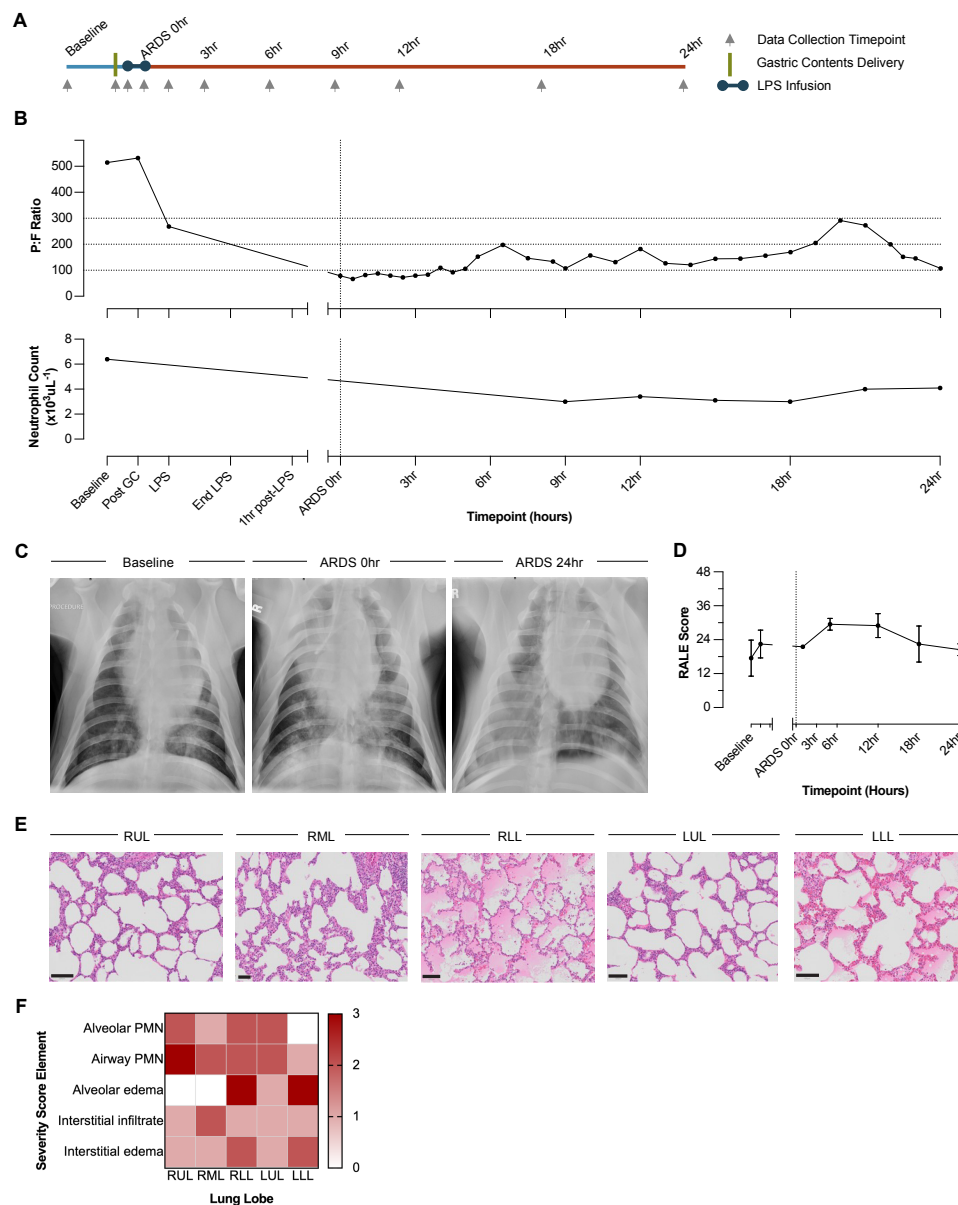


Fig. S8. ARDS 2 - 54456. (A) Experimental timecourse. (B) Pa_O₂:Fi_O₂ ratio over experimental timecourse; neutrophil count (x10³μL⁻¹). (C) Chest radiographs at baseline, ARDS 0hr, and ARDS 24hr. (D) Radiographic Assessment of Lung Edema scores. (E) H&E section from lung tissue at study endpoint. Scale bar = 100 μm. (F) Heatmap of lung injury severity score by score element and lung lobe. GC = gastric contents, LPS = lipopolysaccharide, RALE = Radiographic Assessment of Lung Edema, RUL = right upper lobe, RML = right middle lobe, RLL = right lower lobe, LUL = left upper lobe, LLL = left lower lobe.

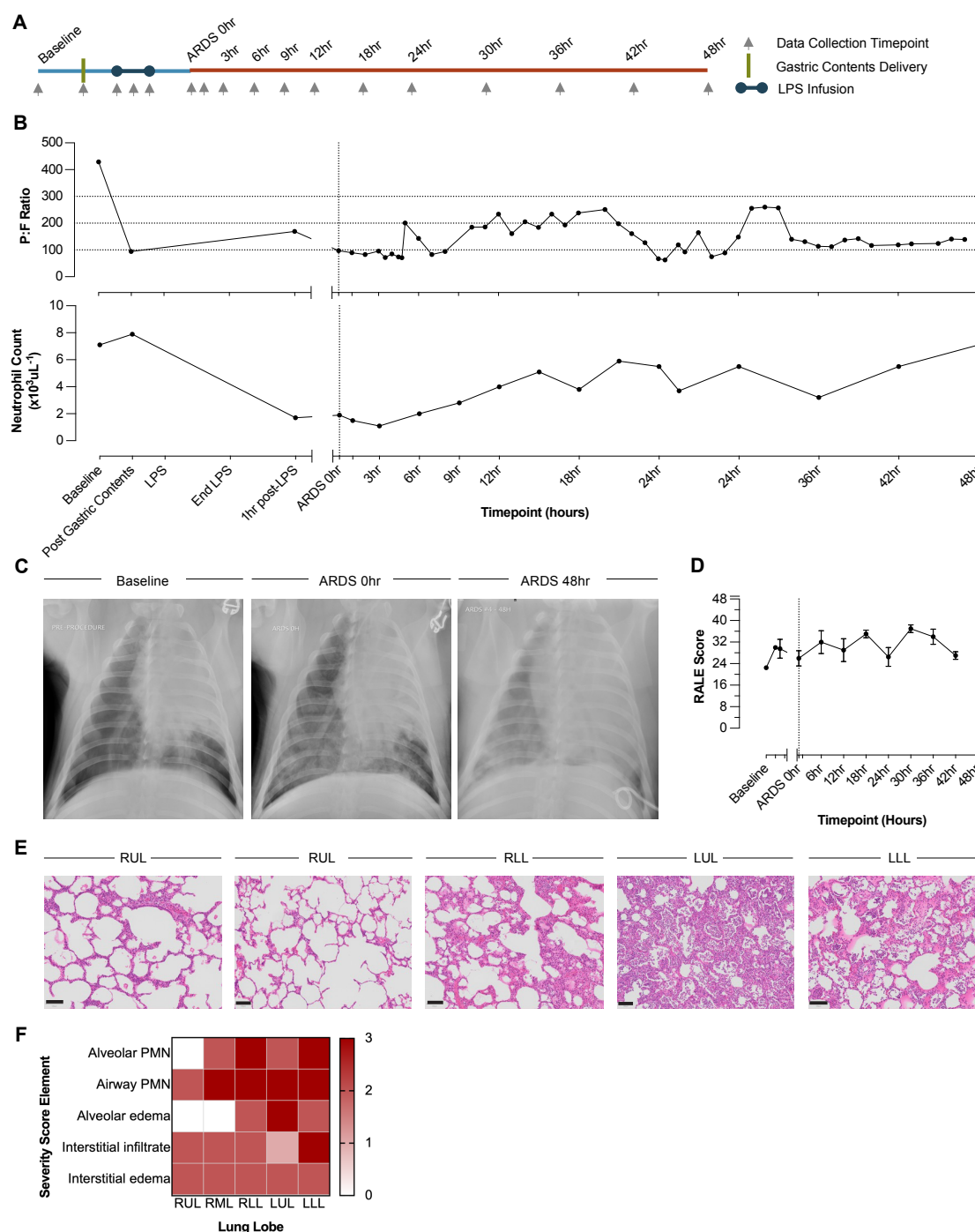


Fig. S9. ARDS 4 - 54659. (A) Experimental timecourse. (B) $\text{Pa}_{\text{O}_2}:\text{FI}_{\text{O}_2}$ ratio over experimental timecourse; neutrophil count ($\times 10^3 \mu\text{L}^{-1}$). (C) Chest radiographs at baseline, ARDS 0hr, and ARDS 48hr. (D) Radiographic Assessment of Lung Edema scores. (E) H&E section from lung tissue at study endpoint. Scale bar = 100 μm . (F) Heatmap of lung injury severity score by score element and lung lobe. GC = gastric contents, LPS = lipopolysaccharide, RALE = Radiographic Assessment of Lung Edema, RUL = right upper lobe, RML = right middle lobe, RLL = right lower lobe, LUL = left upper lobe, LLL = left lower lobe.

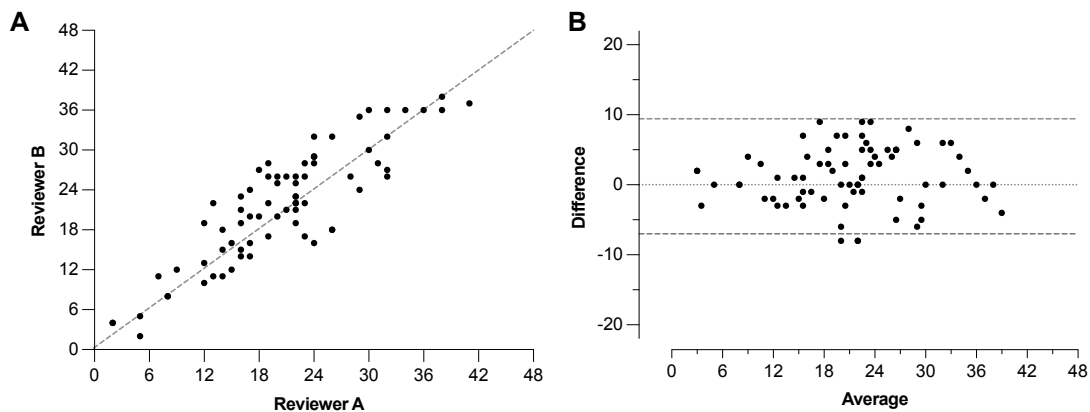


Fig. S10. Agreement on RALE scoring between two independent radiologists. (A) Correlation plot. (B) Bland-Altman plot with average score between two reviewers and difference in score; 95% limits of agreement shown in dashed grey lines. RALE = Radiographic Assessment of Lung Edema scoring

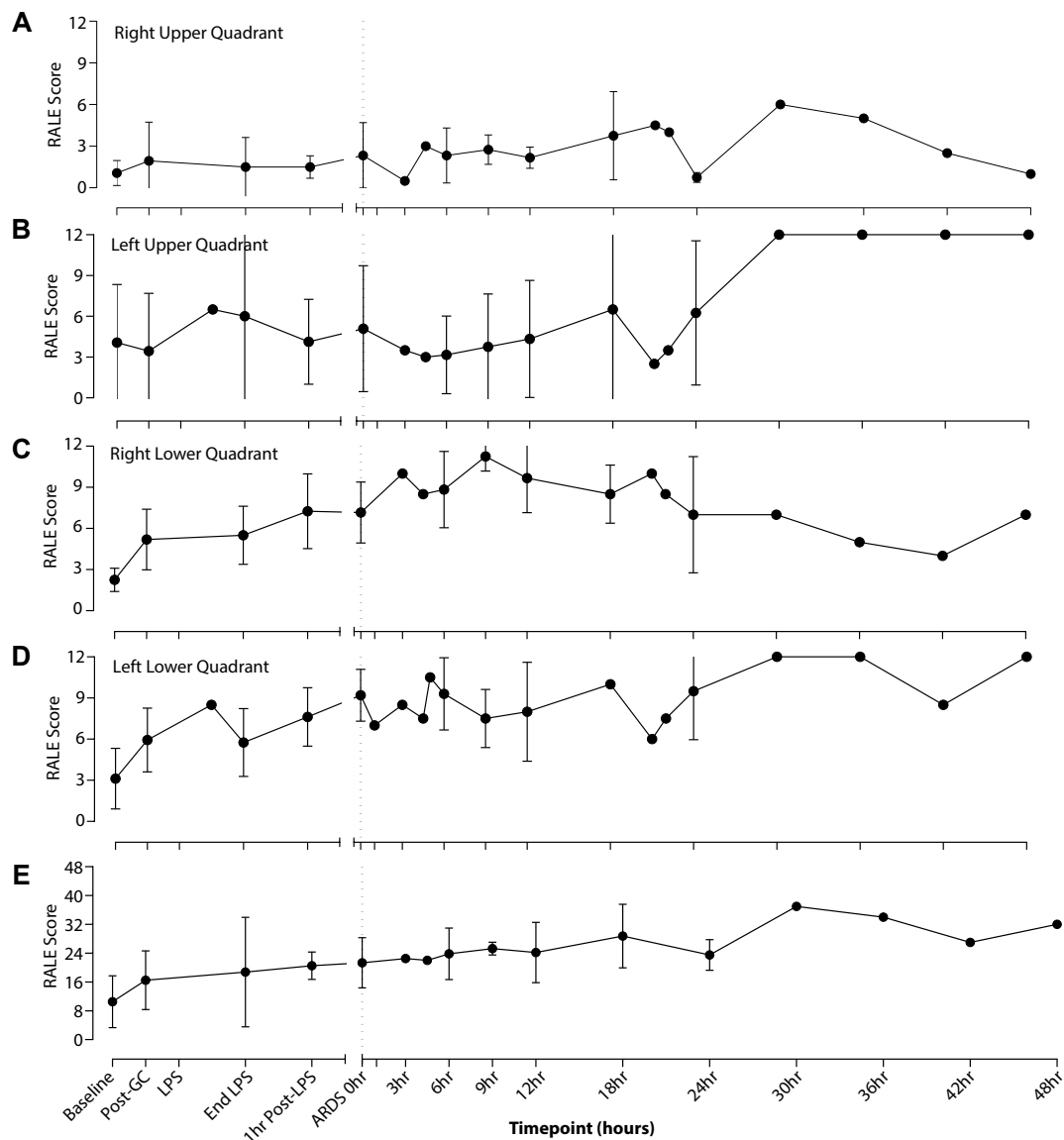


Fig. S11. Radiographic Assessment of Lung Edema scoring from Warren et al. Severity scoring of lung oedema on the chest radiograph is associated with clinical outcomes. Thorax. 2018;73:840-846. (A) RALE score for Right Upper Quadrant; (B) RALE score for Left Upper Quadrant ; (C) RALE score for Right Lower Quadrant ; (D) RALE score for Left Lower Quadrant ; (E) Total RALE Score. GC = Gastric Contents, LPS = Lipopolysaccharides, RALE = Radiographic Assessment of Lung Edema scoring

Table S1. Berlin Criteria from ARDS Definition Task Force, Ranieri VM, Rubenfeld GD, et al. Acute respiratory distress syndrome: the Berlin Definition. JAMA. 2012;307(23):2526-2533.

Timing	Within 1 week of a known clinical insult or new or worsening respiratory symptoms
Chest imaging (CXR or CT)	Bilateral opacities – not fully explained by effusions, lobar/lung collapse, or nodules
Origin of edema	Respiratory failure not fully explained by cardiac failure or fluid overload Need objective assessment (e.g. echocardiography) to exclude hydrostatic edema if no risk factor present
Oxygenation*	
Mild	200 mm Hg < PaO ₂ /F _i O ₂ ≤ 300 mm Hg
Moderate	100 mm Hg < PaO ₂ /F _i O ₂ ≤ 200 mm Hg
Severe	PaO ₂ /F _i O ₂ ≤ 100 mm Hg

*with PEEP ≥5 cm H₂O

Table S2. Baseline measurements of animals

Animal Number	Sex	Age	Weight (kg)	P:F	Arterial Blood Pressure	Pulmonary Artery Pressure	CXR RALE Score
54411	Male	Adult	60.9	516	105/40	Not collected	20.5
54456	Female	Adult	55.4	514	97/60	33/17	17.5
54633	Female	Adult	47	539	106/70	28/17	15.5
54659	Female	Adult	48	429	97/52	36/24	22.5
54990	Female	Adult	45.6	462	122/75	18/10	3
55146	Female	Adult	45	510	100/68	22/12	9
55214	Female	Adult	50	498	104/57	20/12	8
55368	Female	Adult	45	448	104/58	29/15	21
55369	Female	Adult	46.4	543	106/72	19/13	3.5

Table S3. ARDS induction timeline

	Gastric Contents to LPS	LPS Infusion Time	LPS Infusion End to ARDS 0hr
54411	31 min	1 hr	0 hr
54456	3 min	0.5 hr	0 hr
54633	10 min	1 hr	1.5 hr
54659	20 min	1 hr	2.75 hr
54990	20 min	1 hr	0 hr
55146	30 min	1 hr	2.5 hr
55214	35 min	1 hr	4 hr
55369	30 min	1 hr	0 hr
55368	90 min	1 hr	2 hr

Table S4. Higher PEEP/lower FIO₂ ARDSNet ventilator parameters from The Acute Respiratory Distress Syndrome Network. Ventilation with lower tidal volumes as compared with traditional tidal volumes for acute lung injury and the acute respiratory distress syndrome. *N Engl J Med.* 2000;342(18):1301-1308.

F _I O ₂	0.3	0.3	0.3	0.3	0.3	0.4	0.4	0.5	0.5	0.5-0.8	0.8	0.9	1.0	1.0
PEEP (mm H ₂ O)	5	8	10	12	14	14	16	16	18	20	22	22	22	24

Table S5. ELISA information

ELISA	Manufacturer	Catalogue Number	Sample Type	Dilution Factor
C Reactive Protein	Abcam	ab205089	Plasma	1:2000
D-Dimer	LS Bio	LS-F56441	Plasma	1:20
Ferritin	Novus Biologicals	NBP2-7537-1	Serum	1:100

Table S6. Radiographic Assessment of Lung Edema scoring from Warren *et al.* Severity scoring of lung oedema on the chest radiograph is associated with clinical outcomes. *Thorax.* 2018;73:840-846.

Consolidation Score					
Score	0	1	2	3	4
Extent of alveolar opacities	None	<25%	25 – 50%	50 – 75%	> 75%
Density Score:					
Score		1	2	3	
Density of alveolar opacities		Hazy	Moderate	Dense	
Quadrant Score = Consolidation Score x Density Score					
Total Score = Q1 + Q2 + Q3 + Q4					

Table S7. Histopathologic lung injury severity score from Guenthart BA, O'Neill JD, Kim J, et al. Regeneration of severely damaged lungs using an interventional cross-circulation platform. *Nat Commun.* 2019;10(1):1985.

		Airway PMN / hpf			
Score		0	1	2	3
Bronchi and bronchioles (%) containing any neutrophils		0	1-25	26-50	> 50
		Alveolar PMN / hpf			
Score		0	1	2	3
Alveoli (%) more than half-filled with neutrophils		0	1-25	26-50	> 50
		Alveolar edema			
Score		0	1	2	3
Alveoli (%) with edema		< 5	6-25	26-50	> 50
		Interstitial edema			
Score		0	1	2	
Perivascular and peribronchial spaces expanded with edematous fluid		< 5	1x width vessel media	≥ 2x width vessel media	
		Interstitial infiltrate / hpf			
Score		0	1	2	3
Lymphocytes/neutrophils in interstitium around vessels and airways and in alveolar septa and pleura		0	< 50	50-100	> 100

Table S8. Antibodies

PRIMARY ANTIBODIES				
Antibody	Manufacturer	Catalogue Number	Host	Dilution
CD31	Abcam	ab28364	Rabbit	1/50
EpCAM	Abcam	ab71916	Rabbit	1/100
pro-Surfactant Protein C	Abcam	ab90716	Rabbit	1/100
P-Selectin	Abcam	ab202983	Rabbit	1/200
Zonula Occludens-1	Abcam	ab190085	Goat	1/100
Zonula Occludens-3	Abcam	ab205882	Rabbit	1/250
SECONDARY ANTIBODIES				
Fluorophore	Manufacturer	Catalogue Number	Host / Target	Dilution
Alexa Fluor 488	Invitrogen	A-21206	Donkey / Rabbit	1/200
Alexa Fluor 488	Invitrogen	A-21202	Donkey / Mouse	1/200
Alexa Fluor 555	Invitrogen	A-31572	Donkey / Rabbit	1/200
Alexa Fluor 555	Invitrogen	A-31571	Donkey / Mouse	1/200
Alexa Fluor 488	Invitrogen	A-11055	Donkey / Goat	1/200
PRIMARY CONJUGATION KITS				
FITC Conjugation Kit	Abcam	ab188285		
AF555 Conjugation Kit	Abcam	ab269820		
AF647 Conjugation Kit	Abcam	ab269823		

Supplementary Materials and Methods

Preprocedure preparation and hemodynamic monitoring

Swine were vaccinated from the vendor for porcine reproductive and respiratory syndrome, *Mycoplasma hyopneumoniae*, *Haemophilus parasuis*, Swine Influenza (H1N1, H3N2), parvovirus, leptospirosis, *Erysipelas* spp., *E. coli*, *Pasteurella pneumotropica*, and *Bordetella bronchiseptica*. Five days prior to shipment, animals were treated with oxytetracycline (8lb/ton) in food. Animals were housed at Columbia in an AAALAC-accredited facility. All conducted studies were approved by the IACUC at Columbia University.

Swine underwent general anesthesia via intramuscular induction with tiletamine/zolazepam (5 mg kg⁻¹, Zoetis). A 10Fr urinary catheter was placed into the urethra or percutaneously into the bladder, if necessary, to monitor urine output. Peripheral and central venous catheters and arterial catheters were placed percutaneously under ultrasound guidance. A 5Fr introducer (Cook Medical) was placed in the right external jugular vein to establish central venous access for subsequent ECMO cannulation if needed. An 8.5Fr introducer sheath (Arrow) was placed in the left external jugular vein and a 7Fr pulmonary arterial catheter (Edwards) was floated into the pulmonary artery. Placement was confirmed by chest radiograph. A 7Fr dual- or triple-lumen catheter (Arrow) was also placed in the left external jugular vein for medication infusion. A 20G arterial micropuncture kit (Cook Medical) was used to access the femoral artery and subsequently upsized to a 6-7Fr 20cm introducer sheath for continuous arterial blood pressure monitoring, and to establish arterial access for Veno-Arterial (VA)-ECMO, if required. Continuous infusion with vasopressors (norepinephrine 0.125-1.0 mcg kg⁻¹ hr⁻¹, phenylephrine 1 mcg kg⁻¹ min⁻¹, and dopamine 4-6 mcg kg⁻¹ min⁻¹) via central venous catheter was initiated and continued as needed to maintain mean arterial blood pressure \geq 55 mmHg.

Swine were transitioned from isoflurane anesthesia to total intravenous anesthesia utilizing propofol (1-4 mg kg⁻¹ hr⁻¹ or bolus as needed, Zoetis), fentanyl (3-5 mcg kg⁻¹ hr⁻¹, West-Ward), dexmedetomidine (1-5 mcg kg⁻¹ hr⁻¹ or bolus, Zoetis) midazolam (0.1-0.3 mg kg⁻¹ hr⁻¹, Avet Pharma), and/or ketamine (1-5 mg kg⁻¹ hr⁻¹ or bolus, Covetrus). Prior to ARDS induction, a bolus of 100 units kg⁻¹ of heparin sodium (Pfizer) was given and a continuous infusion started at 100 units kg⁻¹ hr⁻¹, titrated to activated clotting time (ACT) of 150-200 (Hemochron). Animals were maintained on 0.9% NaCl, Lactated Ringer's Solution, or 5% dextrose as needed based on fluid balance and blood glucose measurements.

ARDS induction

Gastric aspiration injury was induced by previously established injury methods.¹⁻⁴ Briefly, the tip of a bronchoscope (Ambu® aScope™ 4 Broncho Slim 3.8/1.2) was positioned sequentially 1cm distal to the carina into the right and left mainstem bronchi and standardized gastric contents (30-50 mL; pH 2) were delivered to the bilateral lungs. The location of the tip of the bronchoscope was confirmed visually prior to delivery of gastric contents. After delivery, gastric contents remained in the lungs and bronchial alveolar lavage was not performed to allow development of acute lung injury. Lipopolysaccharide (LPS) from *Escherichia coli* O55:B5 (10 µg kg⁻¹, Sigma) in 100 mL normal saline was infused via central intravenous catheter over 30 to 60 minutes. ARDS 0hr was defined as the timepoint at which the PaO₂/FI₀₂ ratio was first less than 150 mmHg following LPS infusion.

Lung protective ventilation

Initial ventilator settings were tidal volume (TV) 10-12 mL kg⁻¹, positive end expiratory pressure (PEEP) of 5 cmH₂O, respiratory rate (RR) 12-20 breaths min⁻¹, and fraction of inspired oxygen (FI₀₂) of 100%. After ARDS 0hr, ventilator settings were adjusted to ARDSNet parameters (TV 6 mL kg⁻¹, PEEP and FI₀₂ per ARDSNet "Higher FI₀₂" table, and RR titrated to maintain pH > 7.3 with permissive hypercapnia) (**Table S4**). PEEP and FI₀₂ were weaned as tolerated based on pulse oximetry and PaO₂.

Use of paralytics and extracorporeal membrane oxygenation (ECMO)

Pancuronium bromide (initial bolus of 0.1 mg kg⁻¹ followed by continuous infusion of 0.1-0.5 mg kg⁻¹, Hospira) was used for paralysis in animals with severe hypoxia or hypercarbia. Depth of anesthesia was verified by continuous hemodynamic monitoring and vital signs response to painful stimuli every 15 minutes from initiation of paralysis until 2 hours after cessation of the paralytic infusion.

ECMO was used as rescue therapy to attempt to prevent mortality in severely ill swine prior to planned study endpoint. Cannulation for Veno-Venous (VV)-ECMO was achieved via either 20Fr dual-lumen Avalon (Maquet) in the right external jugular vein, or with a 23Fr outflow cannula in the femoral vein and 17Fr inflow cannula in the

right external jugular vein. Veno-Arterial (VA)-ECMO was established with a 23Fr outflow cannula in the REJ and 15Fr arterial cannula in the femoral artery. In all cases, a centrifugal pump (Maquet Rotaflow) was used with an oxygenator and continuous data collection system (Viper).

Blood sample collection

Blood samples were drawn from a femoral arterial line for point-of-care analysis (Epocal). Additional samples were collected in test-specific specimen vials (BD Vacutainer) at predefined timepoints (**Figure 1**) to obtain complete blood count, basic metabolic panel, and liver function tests (Antech Diagnostics). Inflammatory markers (IFN- γ , IL-1 α , IL-1 β , IL-1 α , IL-2, IL-4, IL-6, IL-8, IL-10, IL-12, IL-18, and TNF- α) were analyzed in duplicate by the Discovery Assay Pig Cytokine Array (Eve Technologies). Other markers (D-Dimer, C-Reactive Protein, ferritin) were measured by commercially available enzyme-linked immunosorbent assays (ELISAs) per the manufacturer's instructions (**Table S5**).

Radiographic Assessment of Lung Edema (RALE) scoring

Chest radiographs were taken at baseline, following delivery of gastric contents, at ARDS 0hr, ARDS 6hr, ARDS 12hr, ARDS 18hr, ARDS 24hr, ARDS 36hr, ARDS 42hr, and ARDS46-48hr or if clinically indicated. Radiographs were randomly numbered, blinded, and delivered to two radiologists for review without reference to experimental timepoints. Each radiologist independently scored the radiographs based on the Radiographic Assessment of Lung Edema (RALE) which evaluates the extent of consolidation (0 \rightarrow none, 1 \rightarrow <25%, 2 \rightarrow 25-50%, 3 \rightarrow 50-75%, 4 \rightarrow >75%) and density of alveolar opacities (1 \rightarrow Hazy, 2 \rightarrow Moderate, 3 \rightarrow Dense) on a chest radiograph (**Table S6**).⁵ To evaluate reliability of RALE scoring across two independent reviewers, Pearson's correlation coefficient was calculated. A Bland-Altman plot was used to visualize agreement between reviewers.

Experimental endpoint

Pre-defined experimental endpoints were ARDS 6hr ($n=3$) and up to ARDS 48hr. Animals were euthanized prior to experimental endpoint if their clinical status deteriorated despite maximal medical treatment, including vasopressor support, ECMO, and/or cardiopulmonary resuscitation per Advanced Cardiac Life Support, and in consultation with Columbia University Institute of Comparative Medicine veterinarians. Animals were euthanized with an overdose of pentobarbital sodium (100 mg kg⁻¹, Euthasol, Virbac). Death was confirmed via cessation of heartbeat, spontaneous respiration, and lack of corneal reflex by a veterinarian.

Histopathologic analysis of lung injury

Tissue samples were collected from lung segments were immediately fixed in cold phosphate-buffered 4% paraformaldehyde (ThermoScientific) for 24-48 h. Samples were then embedded in paraffin, sectioned at 3 μ m or 5 μ m thickness, and stained with hematoxylin and eosin (H&E) by the Department of Molecular Pathology at Columbia University Medical Center. H&E slides were randomly numbered prior to pathologic review by an experienced pulmonary pathologist under light microscopy without reference to experimental endpoints. Slides from normal swine lung tissue were included within the blinded set of slides for review. A previously described lung injury severity score which includes airway polymorphonuclear cells per high-power field (hpf), alveolar polymorphonuclear cells per hpf, alveolar edema, interstitial infiltrate (lymphocytes and neutrophils in the interstitium around vessels and airways and in alveolar septa and pleura), and interstitial edema (perivascular and peribronchial spaced expanded with edematous fluid) was applied (**Table S7**).¹

Immunohistochemical staining

Lung sections were de-paraffinized, placed in boiling citrate buffer (pH 6.0) for antigen retrieval, and blocked with 10% normal goat serum in phosphate-buffered saline for 2 h at room temperature. Next, primary antibodies were diluted 1:100, applied, and incubated for 12 h at 4 °C or 4 h at room temperature. Secondary antibodies were diluted 1:200 and incubated for 1 h at room temperature. Sections were mounted in Vectashield Mounting Medium with DAPI (Sigma), and coverslips were applied. Images were obtained using an Olympus FSX100 microscope. Immunofluorescence stains for CD31 (Abcam), EpCAM (Abcam), pro-surfactant protein C (Abcam), P-selectin (Abcam), zonula occludens-1 (Abcam), and zonula occludens-3 (Abcam). A complete list of antibodies and dilutions used is provided in **Table S8**.

References

1. Guenthart BA, O'Neill JD, Kim J, et al. Regeneration of severely damaged lungs using an interventional cross-circulation platform. *Nature Communications* 2019 10:1. 2019;10(1):1-16. doi:10.1038/s41467-019-09908-1
2. Meers CM, Tsagkaropoulos S, Wauters S, et al. A Model of Ex Vivo Perfusion of Porcine Donor Lungs Injured by Gastric Aspiration: A Step Towards Pretransplant Reconditioning. *Journal of Surgical Research*. 2011;170(1):e159-e167. doi:10.1016/J.JSS.2011.05.015
3. Fraisse A, Bregeon F, Delpierre S, et al. Hemodynamics in experimental gastric juice induced aspiration pneumonitis. *Intensive Care Medicine* 2006 33:2. 2006;33(2):300-307. doi:10.1007/S00134-006-0457-2
4. Meers CM, de Wever W, Verbeken E, et al. A Porcine Model of Acute Lung Injury by Instillation of Gastric Fluid. *Journal of Surgical Research*. 2011;166(2):e195-e204. doi:10.1016/J.JSS.2010.10.015
5. Warren MA, Zhao Z, Koyama T, et al. Severity scoring of lung oedema on the chest radiograph is associated with clinical outcomes in ARDS. *Thorax*. 2018;73(9):840-846. doi:10.1136/thoraxjnl-2017-211280